Biogeosciences Discuss., doi:10.5194/bg-2017-95, 2017
Manuscript under review for journal Biogeosciences
Discussion started: 4 April 2017

Modelling the diurnal and seasonal dynamics of soil CO_2 exchange in a semiarid ecosystem with high plant-interspace heterogeneity

Jinnan Gong[1], Ben Wang [1,2], Xin Jia[1,2], Wei Feng[2], Tianshan Zha[2], Seppo Kellomäki[1] and Heli Peltola[1]

[1] School of Forest Sciences, University of Eastern Finland, P.O. Box 111, 80101 Joensuu, Finland

[2] Yanchi Research Station, School of Soil and Water Conservation, Beijing Forestry University, Beijing 100083, China

Correspondence to: Jinnan Gong (jinnan.gong@uef.fi)

Abstract

This study represents a first attempt to model the diurnal and seasonal dynamics of soil CO_2 exchange (F_S) in a dryland ecosystem with a high plant-interspace heterogeneity. The modelling used an integrated process-based approach, in which the CO_2 production, transport and surface exchanges (e.g. biocrust photosynthesis, respiration and photodegradation) are considered simultaneously. The model was parameterized and validated with multivariate data measured during year 2013-2014 in a semiarid shrubland ecosystem in Yanchi, northwestern China. We also investigated the sensitivity of simulated F_S to a set of stand-specific parameters and investigated the relative contribution of different flux components. The model explained reasonably well the two-year dynamics of F_S measured from a non-crusted and two lichen-crusted plots. Simulations showed that the temporal pattern of F_S could deviate from that of the total CO_2 production from rooting-zone soil. Such deviations could be explained by the variations of CO_2 dissolution and the CO_2 exchanges of biocrust during wetting-drying cycles, and the root uptake and transport of dissolved CO_2. Moreover, the F_S was spatially sensitive to the plant-interspace differences and the variations in root biomass, soil organic matter and pH. These results emphasized that, the processes beyond autotrophic and heterotrophic respirations and the heterogeneities of soil at plant-interspace can strongly affect the F_S dynamics and their climatic sensitivities. Such variability should be carefully considered in extrapolation of findings from chamber to ecosystem level and from seasonal to inter-annual scales. Based on this work, our model can serve as a useful tool to simulate F_S dynamics in dryland ecosystems.

Keyword: ecosystem modelling; heterogeneity; inorganic carbon; semiarid shrub ecosystem; biocrust

1. Introduction

CO_2 exchange between soil and atmosphere constitutes a major C loss from terrestrial ecosystems (Raich et al., 2002; Giardina et al., 2014). It also plays an important role in the feedbacks between global carbon cycle and climate change (Rustad et al., 2000; Giardina et al., 2014; Karhu et al., 2014). However, the contribution of soil CO_2 flux (F_S) in arid and semiarid (dryland) ecosystems to the global C budget is less-studied (Castillo-Monroy et al., 2011; Gao et al., 2012; Jia et al., 2014), although these areas cover over 40% of land surface and contribute notably to inter-annual variations of terrestrial C sink (Poulter et al., 2014). The temperature dependency of biological CO_2 productions (i.e. autotrophic respiration and heterotrophic respiration) serves a conventional basis for F_S modelling in many terrestrial ecosystems (Raich and Tufekciogul, 2000; Ryan, 2005; Song et al., 2015). Soil CO_2 flux of dryland ecosystems is also widely interpreted using temperature-response functions modified by other environmental constraints, e.g. soil water content, abundances of substrates and microbial activities (Curiel Yuste et al., 2007; Wang et al., 2014a, 2014b, 2015).

Although empirical models may reproduce the dynamics of soil CO_2 flux in specified space-time, their lack of mechanistic descriptions represents a major difficulty in extrapolation under changing environmental conditions (Fan et al., 2015). Soil CO_2 flux is a "bulk" exchange that comprises two main sets of processes, i.e. the CO_2 productions and transport (Fang and Moncrieff, 1999; Fan et al., 2015). Hence, models considering only autotrophic and heterotrophic respiration often fail to account for the observed F_S dynamics (Austin and Vivanco, 2006). Gas transport processes are important mechanisms regulating the magnitude and hysteretic feature of soil CO_2 efflux (Ma et al., 2013). A substantial fraction of respired CO_2 may be transported to atmosphere via xylem, and can't be measured by techniques like soil reparation chambers (Bloemen et al., 2013; 2016). During wet period, soil CO_2 efflux could decrease significantly by water clogging of soil pores, which restricts the diffusion of O_2 and CO_2 gases (Šimunek and Suarez, 1993; Fang and Moncrieff, 1999). In dryland soils, the interactions between CO_2 transport and water cycle could also be intensive, due to the commonly high salinity/alkalinity of soils. Large inorganic C fluxes can be driven solely by dissolution and infiltration of CO_2 and carbonates (Buysse et al., 2013; Ma et al., 2013; Fa et al., 2014). Such inorganic transport may not only contribute to the hourly or diurnal soil CO_2 efflux (e.g. Emmerich, 2003; Xie et al., 2009; Buysse et al., 2013), but also to the terrestrial CO_2 sinks at much broader spatiotemporal scales (Schlesinger, 2009; Li et al., 2015).

Key processes contributing to CO_2 production in dryland soils also extend beyond autotrophic respiration and heterotrophic respiration. Although biocrust organisms (lichens, mosses, bacteria, fungi and microfauna) inhabit in the top few centimetres of the soil profile, they constitute up to 70% of biomes in the plant-interspace (Belnap, 2003). These communities are able to uptake C from the atmosphere (Belnap, 2003; Castillo-Monroy et al., 2011; Maestre et al., 2013), leading to largely

Biogeosciences Discuss., doi:10.5194/bg-2017-95, 2017
Manuscript under review for journal Biogeosciences
Discussion started: 4 April 2017

greater concentration of organic matters in the crusted layer than the sub-soils (Ciais et al., 2013). Although crust organisms could maintain inactive under stresses (e.g. drought, Green and Proctor, 2016), their photosynthetic potential could be large (Zaady et al., 2000; Lange, 2003), even comparable to temperate forests with closed canopies (e.g. Zaady et al., 2000). The net C uptake by biocrust is highly sensitive to stresses like droughts, thermal extremes and excessive ultraviolet radiation (Pointing and Belnap, 2012). Such variations can readily alter the crusted soils between considerable CO_2 sinks and sources within a few hours (e.g. Bowling et al., 2011; Feng et al., 2014). In addition, the accumulation of debris from crust and canopy further fuels photodegradation, which represents an important abiotic C loss in arid conditions beside the biotic decomposition (e.g. Austin and Vivanco, 2006). Photodegradation is likely to dominate the mineralization during dry daytime period, when the radiation is strong and microbial activities are prohibited by low moisture content and high temperature (e.g. Gliksman et al., 2016). On an annual basis, photodegradation could consume more than 10% of soil organic matter (SOM) at surface (e.g. Austin and Vivanco, 2006; Henry et al., 2008; Brandt et al., 2010). This could be the case even for the substrates (e.g. lignin) that are difficult to degrade via biotic pathways (Henry et al., 2008).

The influences of multiple C processes (i.e. autotrophic and heterotrophic respiration, net C uptake by biocrust, inorganic C fluxes and photodegradation) on soil CO_2 exchange are highly overlapped and tightly related to the water-energy processes. In dryland ecosystems, patchy vegetation and large fractions of interspace are common features (Domingo et al., 2000), and the water-thermal conditions can vary considerably from plant cover to interspace even within a few meters (Rodríguez-Iturbe et al., 2001; Caylor et al., 2008; Ma et al., 2011). The water-energy dynamics at the different surfaces are linked by multiple advection processes both above- and below-ground (Gong et al., 2016). Due to the complexity of water-energy processes, there may exist possibly high non-linearity of water-thermal responses to the climatic variability (e.g. Phillips et al., 2011; Barron-Gafford et al., 2013). This will also complicate the C responses and consequently affect the relationships between the CO_2 fluxes and environmental controls (e.g. Jarvis et al., 2007; Song et al., 2015).

The global change is expected to increase annual mean air temperature considerably and change precipitation regimes (Donat et al., 2016). Understanding the response of dryland ecosystems to such changes requires mechanistic models that integrate the multiple biotic and abiotic mechanisms in soil C cycling. So far, only a few models have coupled the biotic CO_2 productions with the transport of gas and heat (Šimunek and Suarez, 1993; Fang and Moncrieff, 1999; Phillips et al., 2011; Ma et al., 2013; Fan et al., 2015). Nevertheless, none of those models have described the heterogeneous water-energy processes in soil-vegetation-atmosphere continuum (SPAC), or the unconventional C fluxes such as net C uptake by biocrust and photodegradation despite the importance of these processes in arid and semiarid environments. Models by Porada et al. (2013) and Kinast et al. (2016) represent the few existing work in this sense. However, both models focus on the patterns at the regional-scale with very simplified ecosystem processes and neglect stand-scale heterogeneities of water-energy budget, and have not yet been validated by field measurements.

This study represents a first attempt to model the diurnal and seasonal dynamics of soil CO_2 exchange (F_S) in a dryland ecosystem with a high plant-interspace heterogeneity. The modelling used an integrative process-based approach, in which the CO_2 production, transport and surface exchanges (e.g. biocrust photosynthesis, respiration and photodegradation) are considered simultaneously. The model was parameterized and validated by multi-variant data measured during year 2013-2014 in a semiarid shrubland ecosystem in Yanchi, northwestern China. By employing the model, we also investigated the sensitivity of simulated F_S to a set of stand-specific parameters and investigated the role of different flux components in regulating the F_S. The model development in this study is based a water-energy modelling by Gong et al. (2016).

2. Materials and methods

2.1 Outlines for the modelling

The process-based modelling was based on multi-variate data measured during year 2013-2014 in a semiarid shrubland ecosystem located at the southern edge of the Mu Us desert (37°42'1" N, 107°13'7" E, 1560 m above sea level), Ningxia, northwestern China (see Wang et al., 2014a, 2015). The long-term mean temperature (1954–2004) is 8.1 °C, and the mean annual precipitation is 287 mm, most of which falls from July to September (Jia et al., 2014). The radiation and evaporation demand are high in this area, i.e. the annual incoming shortwave radiation is 1.4×10^5 J cm^{-2} and the annual potential evaporation is 2024 mm. The vegetation is dominated by scattered crowns of *Artemisia ordosica* (Fig. 1a). The soil is highly alkaline (pH = 8.2). Biocrust (mainly lichens and algae) covers about 40% of interspace soil. The thickness of the crust layer was 0.5 – 2.5 cm (Gong et al., 2016).

The modelled ecosystem was subtracted as replications of “representative land units" (RLU, Fig. 1; Gong et al., 2016), which consist of the area covered by shrubs and the surrounding soil (interspace). Vertically, the model simulates the C flows over the soil profile and the water-energy transport from the lower boundary of rooting zone to a reference height in the boundary atmosphere. Horizontally, the SPAC processes at plant cover and the surrounding interspace are differentiated but related via advection and diffusion flows, as driven by the gradients of temperature, water potential and gas concentrations. The mineralization, uptake and transport of soil C and N are further regulated by water-energy conditions. Key processes and variables included in the FS modelling are shown in Fig. 1(c).

The model includes a set of sub-models, which describe: (i) CO_2 dissolution, transport and efflux; (ii) Autotrophic and heterotrophic CO_2 productions in the soil profile; (iii) CO_2 uptake and emission by biocrust; (iv) Surface energy balance and soil temperature profile; and (v) Soil hydrology and

Biogeosciences Discuss., doi:10.5194/bg-2017-95, 2017
Manuscript under review for journal Biogeosciences
Discussion started: 4 April 2017

water balance. These sub-models are linked by multiple feedbacks to represent the coupling of C, water, vapor and energy transportations in the ecosystem. Sub-models (iv) - (v) have been developed and described in details in our previous work (Gong et al. 2016), which focused on (i) introducing the plant-interspace heterogeneity into water-energy modelling, and (ii) investigating the influences of such heterogeneity on the ecosystem water-energy budgets for a dryland ecosystem. Gong et al. (2016) also validated the model in regard to the diurnal to seasonal dynamics of radiation balance, surface energy balance, soil temperature and moisture content in the footprint area of a eddy-covariance (EC) site (details of measurement see Jia et al., 2014). In this work, we therefore focus on the development of sub-models (i) – (iii) and their parameterization and validation by F_S measurements, based on automatic respiration chambers from crust-covered and non-crusted soils. Based on the validated model, we also analyzed the model sensitivities to stand parameters and plant-interspace heterogenity and investigated the relative contribution of different flux components to F_S.

2.2 Modelling approaches

2.2.1 Submodel (i): CO_2 transport, dissolution and efflux

For soil fraction *x* (see Fig. 1b for RLU settings), CO_2 exchange (F_S, upward positive) was the sum of CO_2 exchange by biocrust (F_B), photodegradation (F_P) and the total emission from soil under the biocrust layer (F_T):

$$F_{S_x} = F_{B_x} + F_{T_x} + F_{P_x} \tag{1}$$

where F_B is the net balance between biocrust photosynthesis (P_B) and respiration (R_B), and F_B = P_B – R_B (see Section 2.2.3). F_T was modelled based on the mass-balance functions of PATCIS (Fang and Moncrieff, 1999), which combined major transport processes in both gaseous and liquid phases. To account for the plant-interspace heterogeneity, we expanded the original one-dimensional function to the two-dimensional space. For soil layer (*x*, *i*) and time step *t*, the CO_2 concentration and C flows were calculated as follows:

$$\frac{\partial C_{x,i}}{\partial t} = \frac{\partial}{\partial z}\left(F_{dg}^{v} + F_{ag}^{v} + F_{dw}^{v} + F_{aw}^{v}\right) + \frac{\partial}{\partial h}\left(F_{dg}^{h} + F_{ag}^{h} + F_{dw}^{h} + F_{aw}^{h}\right) + S_{x,i} \tag{2}$$

where superscripts *v* and *h* denote the vertical and horizontal directions, respectively (see also in Gong et al., 2016); *C* is the total CO_2 content; F_{dg} and F_{dw} are the CO_2 flows due to diffusion/dispersion via the gaseous and liquid phases; F_{ag} and F_{aw} are the flows in gaseous and liquid phases due to gas convection and water movement, and *S* is the net CO_2 sink of the layer. The calculation schemes of F_{dg}, F_{dw}, F_{ag} and F_{aw} have been described in detail by Fang and Moncrieff (1999). F_T is the total exchange of gaseous CO_2 between surface and topmost layer:

$$F_{T_x} = F_{dg_{x,1}}^{v} + F_{ag_{x,1}}^{v} + E_{x,1}^{S} C_{w_{x,1}} \tag{3}$$

where $E^S_{x,1}$ is the soil evaporation at section x (see Eq. (17) in Gong et al., 2016); C_w is the equivalent CO_2 concentrations in the solution of the topmost soil. For layer (x, i), C_w is linked to the gaseous CO_2 concentrations (C_g):

$$C_{x,i} = Cg_{x,i}(V_{x,i} - \theta_{x,i}) + Cw_{x,i}\theta_{x,i} \quad (4)$$

where V is the total porosity; and θ is soil water content.

C_g and C_w were further related via the dissolution-dissociation balance of CO_2 in soil solution, following Fang and Moncrieff (1999) and Ma et al (2013):

$$CO_2(g) + H_2O(l) \rightleftarrows H_2O(l) + CO_2(aq) \qquad K_H = P_C/CO_2^{aq} \quad (5)$$

$$CO_2(aq) + H_2O(l) \rightleftarrows H_2CO_3 \qquad K_0 = CO_2^{aq}/[H_2CO_3] \quad (6)$$

$$H_2CO_3 \rightleftarrows [H^+] + [HCO_3^-] \qquad K_1 = [H^+][HCO_3^-]/[H_2CO_3] \quad (7)$$

$$HCO_3^- \rightleftarrows [H^+] + [CO_3^{2-}] \qquad K_2 = [H^+][CO_3^{2-}]/[HCO_3^-] \quad (8)$$

where P_C is the partial pressure of CO_2 in pore air; K_H is Henry's Law constant; K_0, K_1 and K_2 are equilibrium coefficients of dissolution, the first- and the second-order dissociation reaction for carbonic acid, respectively (for details see Fang and Moncrieff, 1999). The equilibrium $[H^+]$ was determined by the soil pH and the coefficients K_H, K_0, K_1 and K_2, which were functions of soil temperature in each soil layer (Fang and Moncrieff, 1999). Cw was calculated as the sum of CO_2^{aq}, H_2CO_3, HCO_3^- and CO_3^{2-}.

2.2.2 Submodel (ii): autotrophic and heterotrophic CO_2 productions along the soil profile

For soil layer (x, i), $S_{x,i}$ (Eq. 2) was calculated as the sum of autothrophic and heterotrophic CO_2 productions, and the dissolved CO_2 removed with the water uptaken by roots:

$$S_{x,i} = Rs_{x,i} + Ra_{x,i} - E_{x,i}Cw_{x,i} \quad (9)$$

where E is the transpirative uptake of water (Gong et al., 2016); Rs is the CO_2 production by heterotrophic SOM decomposition; Ra is the autotrophic respiration of the rhizosphere, which comprises maintenance respiration (Rm) and growth respiration (Rg):

$$Ra_{x,i} = Rm_{x,i} + Rg_{x,i} \quad (10)$$

To simulate Rs, we simplified the pool-type model of Gong et al (2013, 2014), which was originated from Smith et al (2010) for simulating coupled C and N cycling in organic soils. SOM pool in each soil layer was divided into debris (M_{deb}, i.e. litters from roots and biocrust), microbes (M_{mic}) and humus (M_{hum}), which are different in biochemical recalcitrance and N content. During decaying, mineralized masses transfer from M_{deb} and M_{mic} to more resistant form (i.e. M_{hum}), leading to a decrease in lability (e.g. Li et al., 1992). The mineralization of organic C followed first-order kinetics and was constrained by multiple environmental multipliers, including temperature, water content and oxygen content (Šimunek and Suarez, 1993; Fang and Moncrieff, 1999):

$$m_{x,i}^{r} = M_{x,i}^{r} k_r f(Ts_{x,i}) f(\theta_{x,i}) f(O_{x,i}) dt \quad (11)$$

where superscript r denotes the type of SOM pool (r=1 for M_{deb}, r=2 for M_{mic}, and r=3 for M_{hum},); m is mineralized SOM during time step dt; k is the decomposition constant; dt is time step; $f(Ts_{x,i})$, $f(\theta_{x,i})$ and $f(O_{x,i})$ are multiplier terms regarding the temperature, water content and oxygen restrictions, respectively. $f(O_{x,i})$ was calculated following Šimunek and Suarez (1993). $f(Ts_{x,i})$ and $f(\theta_{x,i})$ were reparameterized with respect to the site-specific conditions of plants and soil (see Section 2.3.4). The CO_2 production from mineralization was further regulated by the N-starvation of microbes following Smith et al. (2010):

$$Rs_{x,i} = r_E m_{x,i}^{r} \quad (12)$$

where r_E is the gas production rate ($r_E \epsilon$ [0, 1]), and (1- r_E) is the proportion of organic matters passed to the downstream SOM pools. The evolution of each SOM pool was calculated as below:

$$M_{x,i}^{r} = (1 - r_E) m_{x,i}^{r-1} - m_{x,i}^{r} + A_{x,i}^{r} dt \quad (13)$$

where A is the SOM input rate (A=0 for M_{mic} and M_{hum}); superscript r-1 denotes the source SOM pools.

$Rm_{x,i}$ was calculated in a similar way to $Rs_{x,i}$ (e.g. Chen et al., 1999; Fang and Moncrieff,1999). $Rg_{x,i}$ was calculated as a fraction of photosynthetic assimilates, following Chen et al. (1999):

$$Rm_{x,i} = M_{x,i}^{R} k_R f(Ts_{x,i}) f(\theta_{x,i}) f(O_{x,i}) dt \quad (14)$$

$$Rg_{x,i} = k_g P_g fr_{x,i} \quad (15)$$

where M^R is the root biomass; k_R is the specific respiration rate of roots; k_g is the fraction of photosynthetic assimilate consumed by growth respiration; $fr_{x,i}$ is the mass fraction of roots in soil layer (x, i). P_g is the photosynthesis rate of plants. P_g was estimated using a modified Farquahar's leaf biochemical model (see Chen et al., 1999). This model simulates photosynthesis based on biochemical parameters (i.e., the maximum carboxylation velocity, V_{max}, and maximum rate of electron transport, J_{max}), foliage temperature (Tc) and stomatal conductance (gs). The values of V_{max} and J_{max} were obtained from in situ measurements from the site (Jia et al., unpublished). Tc and gs were given in the energy balance sub-model, which was detailed in Gong et al. (2016).

N content bonded in SOM mineralized and was added to soil layers simultaneously with decaying. The abundance of mineral N (i.e. NH_4^+ and NO_3^-) regulates the growth of microbial biomass and r_E following Smith et al. (2010) and Gong et al. (2014). Key processes governing the dynamics of mineral N pools included nitrification-denitrification (Smith et al., 2010), solvent transport with water flows (Gong et al, 2014) and the N uptake by root system. However, the plant growth was not modelled in this work and therefore, N_{upt} was calculated using the steady-state model of Yanai (1994),

Biogeosciences Discuss., doi:10.5194/bg-2017-95, 2017
Manuscript under review for journal Biogeosciences
Discussion started: 4 April 2017

based on the transpiration rate, surface area of fine roots and the diffusion of solvents from pore space to root surface:

$$N_{upt} = 2\pi r_o L \alpha C_o dt \tag{16}$$

where r_o is the fine root diameter; L is the root length, and $2\pi r_o L$ is the surface area of fine roots; α is the nutrient absorbing power, which denotes the saturation degree of solute uptake system ($\alpha \in [0,1]$); C_o is the concentration of solvents at the root surface, and is a function of bulk concentration of mineral N (N_{min}), inward radial velocity of water at the root surface ($v_o = E/(2\pi r_o L)$) and saturation absorbing power α. Further details for calculations of α and C_o can be found in work of Yanai (1994).

2.2.3 Submodel (iii): CO_2 exchange of biocrust and photodegradation

Biocrusts are vertically layered systems that comprise topcrust (or, bio-rich layer) and underlying subcrust (or, bio-poor layer), which are different in microstructure, microbial communities and C functioning (Garcia-Pichel et al., 2016; Raanan et al., 2016). Topcrust is usually few-millimetre thick, which allows the penetration of light and the development of photosynthetic microbes (Garcia-Pichel et al., 2016). On the other hand, the subcrust has little photosynthetic-activity. We here focused mainly on describing the C exchanges in the topcrust, but assumed the C processes in the subcrust were similar to those in the underneath soil. We developed the following functions to describe the C fixation and mass balance in the topcrust,

$$F_{Ct} = P_{Ct} - R_{Ct} \tag{17}$$

where P_{Ct} is the bulk photosynthesis rate; and R_{Ct} is the bulk respiration rate. P_C and R_C were further modelled as follows:

$$P_{Ct} = \frac{\alpha_C A_{PAR} P_{Cm}}{\alpha_C A_{PAR} + P_{Cm}} \tag{18}$$

$$R_{Ct} = M_{Ct} k_{cr} f_{RC}(T_{Ct}) f_{RC}(\theta_{Ct}) \tag{19}$$

where α_C is the apparent quantum yield, P_{Cm} is the maximal rate of photosynthesis, and was a function of the moisture content (θ_{Ct}) and temperature (T_{Ct}) in topcrust; A_{PAR} is the photosynthetically active radiation (PAR); M_{Ct} is the total C in the SOM of topcrust; k_{cr} is the respiration coefficient; $f(\theta_{Ct})$ and $f(T_{Ct})$ are water and temperature multipliers. Here, we assumed no photosynthesis in subcrust. The heterotrophic respiration (R_{Cs}) was calculated as was done for soil respiration (Eq. (11)) based on the C storages ($M^r_{x,1}$) and temperature and moisture content of crust layer (i.e. $Ts_{x,1}$ and $\theta_{x,1}$; see Eq. (29) and Eq. (14) in Gong et al., 2016).

To consider different C losses and exchanges, and to calculate the C balance in topcrust and subcrust, respectively, we considered the following matters. R_{Ct} includes the respirations from both

Biogeosciences Discuss., doi:10.5194/bg-2017-95, 2017
Manuscript under review for journal Biogeosciences
Discussion started: 4 April 2017

autotrophic (M_{CA}) and heterotrophic (M_{CH}) pools. When autotrophic organisms die, SOMs pass from M_{CA} to M_{CH} and influence the turnover processes. A variety of topcrust organisms can reach into subcrust (e.g. through rhizines, Aguilar et al., 2009) and export litters there. When the surface is gradually covered by deposits, topcrust organisms tend to move upward and recolonize at the new surface (e.g. Garcia-Pichel and Pringault, 2001; Jia et al., 2008), leaving old materials buried into the subcrust (Felde et al., 2014). On the other hand, the debris left to soil surface are exposed to photodegradation. Based on above, the C balance in topcrust and subcrust was calculated as following, assuming the partitioning of respiration between autotrophic and heterotrophic pools was proportional to their fractions:

$$M_{Ct} = M_{CA} + M_{CH} \tag{20}$$

$$\frac{dM_{CA}}{dt} = P_{Ct} - R_{Ct}\frac{M_{CA}}{M_{Ct}} - k_m M_{CA} - k_b M_{CA} \tag{21}$$

$$\frac{dM_{CH}}{dt} = k_m M_{CA} - R_{Ct}\frac{M_{CH}}{M_{Ct}} - k_b M_{CH} - F_P \tag{22}$$

$$\frac{dM_{Cs}}{dt} = k_b M_{Ct} - R_{Cs} \tag{23}$$

where k_m is the rate of C transfer (e.g. mortality) from autotrophic pool to heterotrophic pool; k_b is the rate of C transfer (e.g. burying) from topcrust to subcrust; F_P is the loss of SOM due to photodegradation.

Photodegradation tends to decrease surface litter masses in a near linear fashion with the time of exposure (Austin and Vivanco 2006; Vanderbilt et al., 2008). Considering the diurnal and seasonal variations of radiation, F_P was calculated as a function of surface SOM mass and solar radiation:

$$F_{P_x} = M_{surf} k_p Rad_x \tag{24}$$

where Rad_x is the incident shortwave radiation at surface x (Gong et al., 2016); M_{surf} is the surface litter mass; and k_p is the photodegradation coefficient.

2.3 Model parameterization

2.3.1 Measurements of micrometeorology and soil CO_2 efflux

Meteorological variables were measured every 10 seconds and aggregated to half-hourly resolution during 2013-2014. The factors measured included the incoming and outgoing irradiances (PAR-LITE, Kipp and Zonen, the Netherlands), PAR (PAR-LITE, Kipp and Zonen, the Netherlands), air temperature and relative humidity (HMP155A, Vaisala, Finland). Rainfall was measured with a tipping bucket rain gauge (TE525WS, Campbell Scientific Inc., USA) mounted at a nearby site (1 km away, see Wang et al., 2014a). The seasonal trends of the measured *Ta* and *P* can be found in Jia et al. (2016). No surface runoffs were observed at the site, indicating the horizontal redistribution of rainfall was mainly through subsurface flows.

Continuous measurements of F_S were conducted using an automated soil respiration system (model LI-8100A fitted with a LI-8150 multiplexer, LI-COR, Nebraska, USA). The system was on a fixed sand dune of typical size (Wang et al., 2014a), which was located about 1.5 km south from the EC tower described in Gong et al (2016). Three collars (20.3 cm in diameter and 10 cm in height, of which 7 cm inserted into the soil) were installed on average at 3m spacing in March 2012. One collar (C1) was set on a bare soil microsite with no presence of biocrust. Two other chambers (C2 and C3) were set on lichen-crusted soils. F_S was measured hourly from C1 and C2 by opaque chambers, whereas by transparent chamber from C3 to include the photosynthesis and photodegradation. Litters from the shrub canopies were cleared from the collars during weekly maintenance. Hourly *Ts* and θ at 10 cm depth were measured outside each chamber using the 8150–203 soil temperature sensor and ECH2O soil moisture sensor (LI-COR, Nebraska, USA), respectively. Root biomass was sampled near each collar (within 0.5 m) in July 2012, using a soil corer (5 cm in diameter) to a depth of 25 cm. The samples were mixed and sieved sequentially through 1, 0.5 and 0.25 mm meshes, and the living roots were picked by hands. The comparison of the three micro-sites is shown in Table 1. Methods used in data processing and quality control have been described earlier in details (see Wang et al., 2014a, 2015). The quality control led to gaps of 10 - 13% in the F_s dataset.

2.3.2 Parameterization of vegetation and soil texture

The parameterization schemes supporting the simulations of energy balance and soil hydrology in sub-model (i) - (v) have been described previously in detail by Gong et al. (2016). As the water-energy budget is sensitive to vegetation (i.e. canopy size, density and leaf area) and soil hydraulic properties (see Gong et al., 2016), we hereby revalued these parameters for the F_S site. Measurements based on four 5m×5m plots showed that the crown diameter *D* (86 ± 40 cm) and height *H* (47± 20 cm) at this site were similar to those measured from the eddy-covariance (EC) footprint by Gong et al. (2016). However, the shrub density was 50% greater, leading to higher shrub coverage (42%), shorter spacing distance *L* (40.2 cm) and greater foliage area. On the other hand, the subsoil at the F_S site is sandy and much coarser than that at the EC footprint. Therefore, we collected 12 soil cores from 10 cm depth, and measured saturated water content (θ_{sat}), bulk density and residual water content (θ_r) from each sample. Then, the samples were saturated, and covered and drained by gravity. We measured the water content after 2-hour and 24-hour draining, which roughly represented the matrix capillary water content (10 kPa) and field capacity (33 kPa) (Armer, 2011). The shape parameters *n* and α_h (see Eq. (26) in Gong et al. 2016) for the water-retention function were estimated from these values (Table 2).

2.3.3 Parameterization of soil C and N pools

The sizes and quality of soil C pools were parameterized based on a set of previous studies. The total SOC in the root-zone soil (i.e. 60cm depth, bulk density of 1.6 g cm^{-3}) was set to 1200 g m^{-2}, based on the values reported from previous studies in Yanchi area (e.g. Qi et al., 2002; Chen and Duan, 2009; Zhang and Hou, 2012; Liu et al., 2015; Lai et al., 2015). The mass fraction of resistant SOM pool (M_{hum}) was set to 40 - 50 % of total SOM, following work by Lai et al. (2015). The vertical distribution of the SOM pools was described following Shi et al. (2013). At the ecosystem level, the total root biomass was calculated as proportional to the aboveground biomass (Xiao et al., 2005), which linearly related to the crown projection area ($0.5\pi D^2$, Zhang et al., 2008). The vertical profile of root biomass was parameterized following Li and Xiao (2007), and the root biomass was set to decrease with the distance from the center of a shrub crown (Zhang et al., 2008). The N content was parameterized following the measurement of Wang et al. (2015).

Based on the above settings, the specific decomposition rate of debris was estimated from the litterbag experiment of Lai et al. (2015), which showed a 16% decrease in the mass of fine-root litters during a 7-month period of year 2013 at the Yanchi site. The photodegradation coefficient (k_p) was calculated from the mass-loss rate reported by Austin and Vivanco (2006). M_{surf} was set to 33% of M_{CH} in topcrust, assuming the depth of light penetration was about 2 mm and C concentration was homogeneous in topcrust. The surface litter from canopy was not considered in this modelling, as the plant litters were cleaned from the collars during weekly maintenance. The specific respiration rate of roots (k_R), however, could be much greater during vegetative growing stage than other periods, e.g. at the defoliation stage (Fu et al., 2002; Wang et al., 2015). Here we linked k_R to the development of foliage in modelling using the approach of Curiel Yuste et al. (2004):

$$k_R = k_{R0}(1 + n_R L_l / L_{max}) \tag{25}$$

where k_{R0} is the "base" respiration rate (Table 2); L_l is the green leaf area, which is a function of Julian day (Gong et al., 2016); L_{max} is the maximum L_l; n_R is the maximum percentage of variability and is set to 100%.

2.3.4 Parameterization of the water-thermal sensitivity of soil CO_2 productions

Based on the empirical study of Wang et al. (2014a), the steady-state sensitivity of CO_2 productions to soil temperature and water content (i.e., $f(Ts)f(\theta)$, Eq. (11)) can be described as a logistic-power function:

$$f(Ts)f(\theta) = f(Ts,\theta) = \{1 + \exp[a(b - Ts)]\}^{-1}(\theta/\theta_{sat})^c \tag{26}$$

where *a*, *b* and *c* are empirical parameters. This function represents the long-term water-thermal sensitivity of CO_2 productions over the growing seasonal, yielding an apparent temperature sensitivity Q_{10} of 1.5 for the emitted CO_2 (Wang et al. 2014a). However, this could underestimate the short-term sensitivities of CO_2 productions. The apparent Q_{10} could be much greater at the diurnal level than at the seasonal level (Wang et al., 2014a). In this work, we firstly calculated the "base" sensitivity using the long-term scheme (Eq. 26) with 1-day moving average of water-thermal conditions. Then the deviation of hourly sensitivity from "base" condition was adjusted by the short-term Q_{10}:

$$f(Ts)f(\theta) = f(Ts_{short}, \theta_{short}) + [f(Ts, \theta) - f(Ts_{short}, \theta_{short})]Q_{10}{}^{(Ts-Ts_{short})/10} \quad (27)$$

$$Q_{10} = \max\left[Q_{10}(Ts_{short}), Q_{10}(Ts_{short})\right] \quad (28)$$

$$Q_{10}(Ts_{short}) = -0.42\, Ts_{short} + 12.4 \quad (29)$$

$$Q_{10}(Ts_{short}) = 18010\, \theta_{short}{}^{3.721} + 1.604 \quad (30)$$

where Ts_{short} and θ_{short} are the 1-day moving averages of Ts and θ, respectively; Q_{10} (Ts) and Q_{10} (θ) are the adjustment functions for short-term apparent Q_{10}, regarding the short-term Ts and θ.

Further non-linearity of soil respiration responses refers to the rain-pulse effect (or the "Birch effect", Jarvis et al. 2007), that respiration pulses triggered by rewetting can be orders-of-magnitudegreater than the value before rain event (Xu et al., 2004; Sponseller, 2007; Cable et al., 2013). Such response could be very rapid (e.g. within 1 hour to 1 day, Rey et al. 2005) and sensitive to even minor rainfalls. It also seems that the size and duration of a respiration pulse not only depend on the precipitation size, but also on the moisture conditions prior to the rainfall (Xu et al., 2004; Rey et al., 2005; Evans and Wallenstein, 2011). In this work, we multiplied a simple rain-pulse coefficient (f_{pulse}) to Eq. (26):

$$f_{pulse} = max[1, (\theta/\theta_{72h})^{n_p}] \quad (31)$$

where is the 3-day moving average of soil moisture content; n_p is a shape parameter and was set to 2 in this study. θ_{72h} is the 72-hour moving average of θ.

2.3.5 Parameterization of biocrust photosynthesis and respiration

In sub-model (iii), Equations (17) - (19) were parameterized based on the experiment of Feng et al. (2014). In the experiment, 50 lichen (topcrust) samples of 0.5-0.7 cm thickness (100% coverage, average C content of 1048 umol C cm^{-3}) were collected from a 20 m × 20 m area. The samples were wetted and incubated under controlled T_{Ct} (i.e. 35°C, 27°C, 20°C, 15°C, and 10°C). These samples were divided into two groups to measure the net primary productivity (NPP) and dark respiration (Rd) separately. Gas exchanges and light response curve for each crust sample were measured using LI-6400 infrared gas analyzer equipped with an LI-6400-17 chamber and an LI-6400-18 light source (LI-

COR, Lincoln, NE, USA). Measurements were taken at ambient CO_2 values of 385 ± 35 ppm. Saturated topcrust samples were placed in a round tray and moved to the chamber. CO_2 exchange was measured during the drying of samples, until the CO_2 flux diminished. During drying, θ_{Ct} was measured every 20 min. For more details see Feng et al. (2014).

Fitting the measured Rd to T_{Ct} and θ_{Ct} (see Fig. 2a) obtained the multipliers in Eq. (19) as following:

$$f_{RC}(T_{Ct})f_{RC}(\theta_{Ct}) = Q_{Ct}^{\frac{(T_{Ct}-20)}{10}}(a_{RC} + b_{RC}\theta_{Ct} + c_{RC}\,{\theta_{Ct}}^2) \quad (32)$$

where Q_{Ct}, a_{RC}, b_{RC}, c_{RC} are the fitted shape parameters (Table 2).

The parameterized Eq. (19) was then used to simulate the Rd for the NP samples, based on the correspondent T_{Ct} and θ_{Ct} of each measurement. P_{Cm} was determined by subtracting the simulated respiration rate from the NP measured under light-saturated conditions. Then P_{Cm} was fitted to T_{Ct} and θ_{Ct} as following (Fig. 2b):

$$P_{Cm} = f_{Pt}(T_{Ct})\,f_{Pw}(\theta_{Ct})$$

$$= \left(a_{Pt} + b_{Pt}T_{Ct} + c_{Pt}\,{T_{Ct}}^2 + d_{Pt}\,{T_{Ct}}^3\right)\left(-a_{Pw} + b_{Pw}\theta_{Ct} - c_{Pw}\,{\theta_{Ct}}^2 + d_{Pw}\,{T_{Ct}}^3\right) \quad (33)$$

where a_{Pt}, b_{Pt}, c_{Pt}, d_{Pt}, a_{Pw}, b_{Pw}, c_{Pw}, d_{Pw} are fitted shape parameters (Table 2).

It should be addressed that T_{Ct} and θ_{Ct} could change more rapidly than the mean conditions of the crust (i.e. $Ts_{x,1}$ and $\theta_{x,1}$). In this work, T_{Ct} was calculated from the surface temperature (T_x, see Eq. (13) in Gong et al., 2016) and $Ts_{x,1}$ by linear interpolation. The calculation of θ_{Ct}, on the other hand, depended on the drying-rewetting cycle. During drying phases, θ_{Ct} was interpolated linearly from $\theta_{x,1}$ and surface moisture content (θ_x); whereas during wetting phases, the mass balance of water input P and evaporation loss ($E^s_{x,1}$, see Eq. (17) in Gong et al., 2016) was considered:

$$T_{Ct} = \frac{T_x Z_{Ct} + Ts_{x,1} Zs_{x,1}}{Z_{Ct} + Zs_{x,1}} \quad (34)$$

$$\theta_{Ct} = max\left[\frac{\theta_x Z_{Ct} + \theta_{x,1} Zs_{x,1}}{Z_{Ct} + Zs_{x,1}}, \theta_{Ct} + \frac{P - E^S_{x,1}}{Z_{Ct}}\right] \quad (35)$$

where $Zs_{x,1}$ is the thickness of the biocrust; and Z_{Ct} is the thickness of the topcrust. θ_x was calculated from the surface humidity and the water retention of the crust layer, using Eq. (25) – (26) by Gong et al. (2016).

2.3.6 Calculation of litter input to soil and SOC transport in biocrust

The litter falls added to each soil layer ($A^1_{x,i}$, Eq. (13)) were linked to the mortality of roots, which was calculated following Asaeda and Karunaratne (2000).

Biogeosciences Discuss., doi:10.5194/bg-2017-95, 2017
Manuscript under review for journal Biogeosciences
Discussion started: 4 April 2017

$$A_{x,i}^{1} = k_{mo} {Q_{mo}}^{Ts_{x,i}-20} M_{x,i}^{R} \quad (36)$$

where k_{mo} is the optimal mortality rate at 20ºC; Q_{mo} is the temperature sensitivity parameter (Asaeda and Karunaratne, 2000). Similarly, we attributed the C transport rate (A_{Cm}) from M_{CA} to M_{CH} mainly to the mortality of autotrophic organisms. We assumed that most mortality of crust organisms occurred during abrupt changes in wetness, as microbial communities may adapt slow moisture changes or remain inactive during drought (e.g. Roberson and Firestone, 1992; Reed et al., 2012; Coe et al., 2012; Garcia-Pichel et al., 2013; Maestre et al., 2013). Here, we introduced a water-content multiplier, $f_m(\theta_{Ct})$, to describe the impact of abrupt θ_{Ct} changes on k_m:

$$A_{Cm} = k_{mc} {Q_{mo}}^{T_{Ct}-20} f_m(\theta_{Ct}) M_{CA} \quad (37)$$

$$f_m(\theta_{Ct}) = \max[0.01, 1 - \min(\theta_{Ct}, \theta_{Ct7})/\max(\theta_{Ct}, \theta_{Ct7})] \quad (38)$$

where k_{mc} is the optimal mortality rate at 20ºC; Q_{mo} is the temperature sensitivity parameter (Asaeda and Karunaratne, 2000); θ_{Ct7} is the forward 7-day moving average of θ_{Ct}.

C transport from topcrust to subcrust was calculated as driven mainly by the sand deposition and burying of topcrust SOM. Assuming the C content in topcrust was homogeneous and the thickness Z_{Ct} was near-constant, the transport rate (k_b) was then proportional to the sand deposition rate:

$$k_b = \frac{k_{sand}}{\rho_{bulk}} \frac{1}{Z_{Ct}} \quad (39)$$

where ρ_{bulk} is the bulk density of soil; k_{sand} is the sand deposition rate in Yanchi area, which is a function of wind velocity (Li and Shirato, 2003):

2.4 Model validation and sensitivity analyses

2.4.1 Boundary conditions and initial values used in model simulations

In the model simulations, soil depth was set to 67.5 cm to cover the rooting zone (Gong et al., 2016), including the crust layer (2.5 cm) and sandy subsoil (65 cm, stratified into 5 cm layers). Water content measured at 70 cm depth was used as the lower boundary condition for hydrological simulation (Jia et al., 2014). The calculation of soil temperature extended to 170 cm depth with no-flow boundary, regarding the probably of strong heat exchange at the lower boundary of rooting zone (Gong et al., 2016). Zero-flow condition was set for the lower boundary of CO_2 and O_2 gases, whereas dissolved CO_2 was able to leech with seepage water. Based on presumed similarity of RLU structures, we assumed no-flux conditions for transports of water, heat, solvents and gases at outer boundary. In the simulation, we assumed instant gas transport via topcrust, whereas considered the CO_2 released by subcrust (R_{Cs}) was subject to the dissolving-transport processes. In this work, we aggregated the C

Biogeosciences Discuss., doi:10.5194/bg-2017-95, 2017
Manuscript under review for journal Biogeosciences
Discussion started: 4 April 2017

processes in subcrust with those in soil profile and set $F_B = F_{Ct}$ (Eq. (2)). The initial ratio of $M_{CA} : M_{CH}$ was set to 2:3. The C concentration of organic matters was set to 50%.

The model simulation employed half-hourly meteorological factors including the incoming shortwave radiation, incoming longwave radiation, PAR, *Ta*, relative humidity, wind speed and precipitation. The initial temperatures and soil moisture content for each soil layer were initialized following the work by Gong et al. (2016). Surface CO_2 concentration was set to 400 ppm. The initial gaseous CO_2 concentration was set to increase linearly with depth (5 ppm cm^{-1}). The initial CO_2 concentration in liquid form was then calculated based on Eq. (4) – Eq. (8). The initial content of mineral N content was set to 40 mg/g, which was within the range of the field observations. The two-dimensional transpirations of water, energy and gases along the soil profile were solved numerically using the Predict–Evaluate–Correct–Evaluate (PECE) method. In order to avoid undesired numerical oscillations, the transport of water, energy and gases were calculated at 5-min sub steps.

2.4.2 Model validation

First, we validated the modelling of soil temperature and moisture content for the F_S site (Test 0). The simulated hourly soil temperature and moisture content at 10 cm depth were compared to the measured values for each collar. The validation was based on the same meteorological data as used by Gong et al. (2016), who validated the model in regard to the diurnal to seasonal dynamics of radiation balance, surface energy balance, soil temperature and moisture content at the EC site.

The validity of the modelled F_S was examined using three separate tests. In Test 1, modelled F_S was validated for non-crusted soils. In this case, F_T in Eq. (1) was the only term affecting F_S (F_B=0 and F_P = 0), and the crust influences on C-water exchanges were excluded. The biocrust-relatedprocesses were considered in Test 2 and Test 3. Test 2 considered the dark respiration of biocrust (R_{Ct}), and set $F_B = R_{Ct}$ and $F_P = 0$. Test 3 considered all the flux components (F_T, F_P and F_B). In these tests, different values of root biomass were assigned to the model regarding the different collar conditions (Table 1). In Test 1 – Test 3, half-hourly F_S were simulated and averaged to hourly values, and compared to the those measured from the collar C1 – C3, respectively. Linear regressions were used to compare the modelled and measured values. The biases (ζ) of the simulated values were calculated by subtracting the measured values from the modelled ones. Gap values in the measurements were omitted in the validation and the bias analyses.

2.4.3 Sensitivity analyses

By employing the validated model, we studied the sensitivity of simulated soil CO_2 efflux to a set of stand-specific parameters and compared the C fluxes at plant-cover and interspace soils (Test 4). This was done to find out how different flux components (i.e. P_{Ct}, R_{Ct}, F_P, F_T, *Ra* and *Rs*) to the soil CO_2

efflux. These simulations were based on model settings for C3 and climatic variables of year 2013-2014. For the comparison purpose, same settings for soil C storages (650 gC m^{-2}), root biomass (200 g m^{-2}) and biocrust were employed at both under-canopy and interspace areas.

Our previous work has already studied the sensitivities of modelled soil temperature and moisture content to the variations in soil texture, water retention properties, vegetation parameters and plant-interspace heterogeneities Gong et al. (2016). In this study, we further tested the sensitivity of the modelled F_S and componential fluxes to the changes in a number of stand-specific variables and parameters (Table 4).

We also investigated the model sensitivities for several newly defined parameters (i.e. n_R, n_p and f_m). It was also studied the sensitivities of modelled C fluxes to the changes in soil temperature and moisture content, which could be biased regarding the heterogeneities of soil texture, hydraulic properties and vegetation covers (see e.g. Ma et al., 2011; Gong et al., 2016). We further on analysed the model sensitivity to a set of biogeochemical parameters, including root biomass, total SOC (M_{tot} = M_{deb} + M_{mic} + M_{hum}) in soil and topcrust (M_{Ct}), soil N content (N_{tot}), ratio of M_{CA} : M_{CH}, the decomposability of debris (k_1), the rates of litter productions from roots (k_{mo}) and topcrust (k_{mc}) and soil pH. Simulated F_S and componential fluxes at the interspace were also compared to the values under no-change conditions.

3. Results

3.1 Model validity

Figure 3 shows the modelled hourly Ts and θ at 10 cm depth with the mean values measured from the F_S site during year 2013. Based on the site-specific vegetation and soil texture parameters, our model explained 97% of the variations in the measured hourly Ts. The model underestimated the temperature mainly in summer time (i.e. day 150-250, Fig. 3a). The underestimation was most pronouncing around the noontime in the diurnal cycle. The measured θ at 10 cm depth was much lower at the F_S site than that shown by Gong et al. (2016) for the EC site (Fig. 3b). Such a difference was in line with the coarser texture of the soil at the F_S site. The model underestimated mainly the soil water content during the freezing season (Fig. 3b). During the ice-free period, it explained 83% of the variations in the measured mean water contents at 10 cm depth.

The measured F_S showed large diurnal and seasonal variations regardless the existence of crust cover (Fig. 4 and Fig. 5). Rain events clearly influenced the hourly F_S measured from the non-crusted surface C1 (Fig. 4a). The F_S dropped significantly from the pre-rainfall level even to near-zero, but rebound rapidly and peaked after rain stopped. Our modelling reasonably reproduced the diurnal and seasonal fluctuations of F_S. The model explained 87 and 83% of the variations in the hourly F_S measured on the non-crusted surface in year 2013 and 2014, respectively (Fig. 4a). The model mainly underestimated the daytime F_S during the freezing seasons. During the ice-free periods, the model overestimated the efflux in early springs. The biases of modelling largely showed a diurnal pattern (Fig. 4c), that F_S was underestimated in noon hours (i.e. from 10 a.m. to 3 p.m.) but overestimated in the afternoon and evening. At the daily level, our model explained 94% of the variations in measured daily efflux during the two-year period (Fig. 4c).

Comparing to the non-crusted surface (C1), the simulated F_S for the crusted surfaces (C2 and C3) exhibited greater deviations from the observations. At the hourly scale, our model explained 75 % (year 2013) and 68 % (year 2014) of the variations of measured F_S from C2 (Fig. 5a), and 68 % (year 2013) and 61 % (year 2014) of the variations of measured F_S from C3 (Fig. 5b). For the two-year period, the root-mean-square errors (RMSE) of the modelled hourly F_S were 0.25 umol m^{-2} s^{-1} and 0.35 umol m^{-2} s^{-1} for C2 and C3, respectively. The biases of the simulated F_S for C2 and C3 showed similar diurnal pattern as compared to C1, and the magnitudes of biases ($|\zeta|$) were greater during the rainfall period (i.e. from the start of raining to 24 hours after end of rainfall) than the inter-rainfall period (Fig. 6). Nevertheless, at the daily scale, the model explained 91% (C2, Fig. 5c) and 86% (C3, Fig. 5d) of the variations in the measured F_S during the two-year period. There were no significant systematic deviations between the measured and the modelled daily values, as indicated by regression slopes close to 1 and intercepts close to 0 (Figs. 4 and 5).

3.2 Model sensitivity

Relative contribution of component fluxes to F_S

If root biomass and SOC were homogeneous at plant cover and interspace, the C loss at interspace was faster than under-canopy on an annual basis (Test 4, Table 3). In both areas, *Rs* was a major contributor to the total CO_2 produced in root-zone soil and F_T dominated the effluxes (F_S) during the two-year period. The simulated NPP of topcrust were 18.2 gC m^{-2} $year^{-1}$ and 31.1 gC m^{-2} $year^{-1}$ at under-canopy and interspace, respectively. At hourly scale, the net C uptake by topcrust could be comparable to F_T after rewetting (Fig. 5A). However, at annual scale, the C losses via respiration and photodegradation accounted for 90% of the GPP, leading to a near-zero contribution of topcrust to F_S during the two year period (i.e. < 5 gC m^{-2} $year^{-1}$).

Test 4 further showed mismatched trends of F_T and the root-zone CO_2 production (R_P). The annual F_T was 17 and 15% smaller than R_P at under-canopy and interspace, respectively. Such a gap was mainly due to the root uptake and transport of dissolved CO_2 (i.e. 36 gC m^{-2} $year^{-1}$) whereas the CO_2 loss via seepages or pore-mediated horizontal flows were limited (i.e. 7.4 gC m^{-2} $year^{-1}$). Moreover, the temporal patterns of F_T and R_P were largely inconsistent with respect to the wetting-drying cycles (Fig. 7a). Comparing to R_P, the responses of F_T to rainfall were largely lagged and smoothed (Fig. 7b – 7d), disregard the size of rain events. R_P increased rapidly following the rewetting of soil. On the other hand, F_T firstly depressed during rainfall then increased after rain ceased. In all the examples, F_T

Biogeosciences Discuss., doi:10.5194/bg-2017-95, 2017
Manuscript under review for journal Biogeosciences
Discussion started: 4 April 2017

exceeded R_P within 48 hours after the ending of rain events. At the annual level, the total R_P was larger during wetting period (i.e. raining days plus 1 day after rainfall) than the rest days of the year (i.e. drying period), whereas the total F_T was greater during the drying period (Fig. 5e).

Sensitivity of modelled F_S to site-specific parameters

In general, the modelled F_S and the component fluxes were more sensitive to ± 2 ºC in *Ts* or ± 10% in θ, comparing to the effects of ± 10% or ± 20% in the other parameters (Table 4). Varying θ by 10% produced greater impacts on the simulated R_P and crust-related fluxes (i.e. P_{Ct}, R_{Ct} and F_P), as compared to changing *Ts* by ± 2 ºC. Increasing θ by 10% enhanced the simulated P_{Ct} and NP_{Ct} of the crust by 41 and 28%, and doubled the annual C sequestration by topcrust. However, such changes in crust C uptake had minor contribution to F_S, as it amounted for only 2.0% of the total efflux.

Adjustment of the newly introduced parameters N_P and f_m by ± 20% produced limited influences on the modelled F_S and the componential fluxes (Table 4). The model was also robust to the adjustment of several crust-related parameters, i.e. k_{mc}, M_{Ct} and M_{CA}: M_{CH}. Comparing to ± 10% in root biomass, varying N_R by 20% led to similar responses in the simulated F_A but much weaker responses in F_T and F_S. A 10% variation in root biomass changed the annual F_T and F_s by about 7%, and such effects were 100% greater than that of 10% changes in the total SOC (M_{tot}).

4. Discussions

4.1 Model performance

Validity of the F_S modelling at non-crusted soil

Our model reasonably well captured the measured dynamics of soil temperature during year 2013, based on revaluing the vegetation and soil hydraulic parameters for the F_S site. The model mainly underestimated the midday temperatures at the collars. In addition, the model underestimated the soil moisture content during the winter freezing period, probably because the impacts of solvents on the thermal conductivity and freezing point of soil water (Viterbo et al., 1999) were not included (see Gong et al., 2016). This could have contributed to the biases in the simulated *Ts* and F_S for freezing period. However, the influences of such biases on annual F_S was marginal, due to the very low emissions during the winter period (see also Liu et al., 2016). During ice-free season, the simulated soil water content agreed well with the measured means, and the biases in the modelled temperature and moisture content were less than the spatial variations observed in the area (e.g. Wang et al., 2015). Therefore, our model could be able to reproduce near-realistic trends for the water-energy conditions at the site. Based on the modelled water-energy dynamics, the model well described the seasonal variations of F_S measured from the non-crusted soil (Test 1) during a two-year period. The model was able to capture the strong variability of hourly/daily F_S in wetting-drying cycles, and the performance was generally better than those based on empirical methods (e.g. Wang et al., 2014a, 2014b). In this

Biogeosciences Discuss., doi:10.5194/bg-2017-95, 2017
Manuscript under review for journal Biogeosciences
Discussion started: 4 April 2017

sense, we assume that our model have included the main mechanisms controlling the F_S dynamics in the non-crusted soil system.

The uncertainties in the modelling, however, may exist in several aspects. *Firstly*, the RLU was a statistical simplification to the target ecosystem at footprint scale (Gong et al., 2016), and may not fully capture the spatially explicitly of soil environment and biogeochemistry at the scale of FS measurements. For example, the model assumed Poisson probability of mutual shading (Bégué et al., 1994), and the probability of shading increased continuously with solar zenith (Gong et al., 2016). However, for explicit space-time, the chance of being sunlit or shaded is more likely to be binary, which possibly explain the underestimation of net radiation (Gong et al., 2016) and the collar temperature around midday, affecting the simulated F_S (see Fig. 3b). Moreover, field observations had considerable spatial variations in soil temperature, water content and biogeochemistry (e.g. pH, litter quality and root biomass) within a distance of 3-5 meters. Such variations could well exceed a magnitude of 10 %, and even over 100 % (e.g. Zhang et al., 2008; Feng et al., 2013; Wang et al., 2015). Therefore, the variation of F_S driven by the spatiality of soil factors could be greater than the responses to ±2 °C in soil temperature or ±10 % in soil water content. Therefore, future modelling may need to consider spatially explicit settings, in order to further minimize the gaps between model settings and the reality, and to improve the reliability of simulated F_S responses to changing climatic conditions.

Secondly, the uncertainties in inorganic C processes could strongly affect the accuracy of modelling, as indicated by the high sensitivity of simulated F_S to soil pH. In this model, the calculation of CO_2 transport was based on gaseous and liquid phases, whereas the solid phase were not involved. This is likely to underestimate the dissolved CO_2 and its fluctuations, regarding the high lime content (2300–5400 kg ha^{-1}) in the soil (Feng et al., 2013; Wang et al., 2015). Based on soil samples of similar lime content (2700 kg ha^{-1}), Buysee et al. (2013) showed that neglecting the inorganic C exchanges of the $CaCO_3$-H_2O-CO_2 system could underestimate F_S during the heating phase of a day, but overestimate F_S during the cooling phase. Such phenomenon was very similar to the diurnal pattern of biases found in our modelling (Fig. 3d). Therefore, further improvement on the modelling may need to consider the solid phase as well. However, the effect of solids could be complicated, as it may differ by the mineral type and degree of exposure to pore air and liquid (Buysee et al., 2013; Fa et al., 2014). Liu et al. (2015) suggested that a considerable fraction of CO_2 absorbed by minerals could even be stored for prolonged period with high biochemical stability. In this sense, the functioning of the CO_2 buffering system may require site-specific parameterizations, in order to improve the model performance at hourly level.

In addition, the current model still lacked mechanistic descriptions on the growth of plants. Comparing to many other ecosystems, drylands feature high root-shoot ratio (Jackson et al., 1996) but low SOC storages. Changes in plant physiology and growth can readily influence root metabolisms and labile SOC pools, thus modify the climatic sensitivities of F_S (Wang et al., 2015). On the other hand, the parameterization of soil respiration employed constant scheme throughout the years. However, the large fluctuation of diurnal and seasonal temperature may drive the microbial communities to shift between warm-adapted to cold-adapted (Van Gestel et al., 2013), which largely enhances winter respiration and its sensitivity to freeze-thaw cycles (Van Gestel et al., 2013; Liu et al., 2016). Both the biotic controls are mixed with the legacy effects of the climatic variability over annual and inter-annual courses (Sala et al., 2012; Jia et al., 2016; Shen et al., 2016), and could affect the C-water simulations cumulatively through the feedbacks between biomass accumulation and soil biogeochemistry (Bradford et al., 2016). This may explain the decrease of model validity from year 2013 to 2014 (Fig. 3, Fig. 4). Therefore, the dynamics of plants and microbial communities are required in future modelling, in order to improve the F_S simulations regarding inter-annual and long-term periods.

Validity of the F_S modelling at lichen-crusted soils

Comparing to the non-crusted soil, the adding of biocrust increased the model uncertainty particularly at the hourly scale (e.g. Fig. 4). The biases of modelled F_S for the lichen-crusted soil mainly exist at hourly level after rewetting. Nevertheless, the model reasonably explained the seasonal dynamics of the measured F_S during 2013-2014, and the RMSE of the modelled hourly F_S was one-order smaller than the seasonal variation of the measured values. This indicated that the model could serve a quantitative tool to simulate seasonal and inter-annual F_S from the lichen-crusted soils in dryland ecosystems similar to the site studied here.

The uncertainty of the F_S modelling for the lichen-crusted soils was partly due to the simulated subsoil processes, as indicated by the similar diurnal patterns of biases across Test 1-3 (Fig. 3, Fig. 5). Other sources of uncertainty may be due to the simulated crust processes, and especially due to the biases of the estimated water content in topcrust (Table 4). The water content in the very thin layer of topcrust can be highly dynamical during wetting-drying cycles. Hence, it is challenging to track the photosynthesis or respiration peaks based on the hourly simulations of micrometeorology and soil hydrology. Moreover, nocturnal water inputs (e.g. dewfalls) often occur at stable atmospheric conditions. These rewetting events are important to the metabolisms of crust organisms (e.g. Liu et al., 2006). However, they are hard to be quantified precisely by EC measurement, or models derived from EC data. These uncertainties further affect together with the biases in the modelling of water-energy balances (Gong et al., 2016). Due to the lack of data on the crust moisture dynamics, it is still difficult to analyse the extent to which such uncertainties could have influenced the model validity.

The challenges to reproduce realistic trends of biocrust C uptake may also relate to the presumed homogeneity of structures of the crust layers and the consistency of C-water processes throughout the simulation. In reality, there may not be clear boundaries between topcrust and subcrust, and even topcrust itself may contain significant variations in microstructure and communities even within one centimetre (Williams et al., 2012; Raanan et al., 2016). Furthermore, the C sequestration of biocrust not only relies on instantaneous environmental factors such as radiation, temperature and water content (Feng et al., 2014), but also depends on the dynamics of microbial communities and their interactions (Belnap, 2003; Pointing and Belnap, 2012; Maestre et al., 2015). The changes in microbial communities, on the one hand, can influence the C functioning of biocrusts directly (Feng et al., 2014; Maestre et al., 2015). On the other hand, such changes affect surface albedo (Chamizo et al., 2012), nocturnal water inputs (Liu et al., 2006), soil aggregate structure and pore forming (Williams et al., 2012; Felde et al., 2014), which ultimately feedback to microniches and water-gas fluxes (Garcia-Pichel et al., 2016). So far, many questions remain unanswered about the mechanisms that control the colonization, adaption and succession of microbial communities and the structure-function of biocrust (Pointing and Belnap, 2012). Further knowledge on these mechanisms will be helpful to improve the modelling of crust C functioning in response to climate change and extreme climatic events.

4.2 Effects of plant-interspace heterogeneity and soil C processes on soil CO_2 effluxes

Clumped distributions of foliage and biomass are critical features for the adaptation and functioning of vegetation in arid and semiarid environments. Previous studies have mainly emphasized the effects of shrub pattern on ecohydrology (e.g. Rongo et al., 2006; Gong et al., 2016) and enrichment of fine sediments and nutrient, known as “resource island” effects (Reynolds et al., 1999; Rietkerk et al., 2004). Our simulations showed that the presence of shrub canopy could also influence the soil C exchanges. Comparing to the interspace, the presence of shrub cover reduced the simulated F_S by 13% annually (Test 4). As the soil SOC and root biomass were set to be the same at under canopy and interspace in the simulation, such a decrease in F_S was probably due to the cooling effect of canopy (Gong et al., 2016) on soil. Such an effect was close to the modelled responses of F_S to ± 2 ºC in soil temperature or ± 10% in soil water content. As the density of roots and litter production are commonly larger under canopy than interspace (e.g. Zhang et al., 2008), the lower respiration rate under canopy tends to facilitate the accumulation of biomass and organic matters in under-canopy soils and feedback to functioning of “resource islands” during prolonged periods. In this context, the different C functioning at plant cover and interspace shall not be neglected in studies on the climatic sensitivity of C dynamics in dryland ecosystems.

Our modelling provide a way to separate the multiple soil C processes and investigate their roles in regulating F_S dynamics in dryland ecosystems. So far, efforts to quantify the soil C loss in terrestrial ecosystems often consider soil C efflux as a synonym of respired CO_2. However, based on this work cautions must be taken when extrapolating the F_S responses from the chamber to ecosystem scale and from short-term to long-term periods. Our simulations reckoned that a considerable fraction of CO_2 produced could be removed by root uptake and leave the volume measured by the respiration chamber. Bloemen et al. (2016) showed that the CO_2 concentration in root xylems could be higher than in soil solutions. This implies that such a “missing source” might be even greater than the model estimation, although our knowledge is still limited about the efficiency of the removal and the diffusion/release of CO_2 during the transport (Bloemen et al., 2016). On the other hand, the soil processes other than autotrophic and heterotrophic respiration could significantly modify the F_S responses to climatic variability. Our simulation highlighted decoupled CO_2 productions and emissions during the wetting-drying cycle, as regulated by the CO_2 transport in soil profile. The simulated CO_2 productions in soil profile were much greater than effluxes during rain pulses (e.g. Fig. 7). This indicated that, the limited FS during rewetting was mainly due to the increased dissolution of CO_2, rather than the reduced respiration rates by low O_2 supply (e.g. Fang and Moncrieff, 1999). This finding is further supported by the measurement of Maier et al. (2011), which showed that 40% of the respired CO_2 could be stored temporally in soil pore-space after rainfalls. The dissolved CO_2 then released gradually with the evaporation of pore water, leading to lagged responses of efflux as compared to respirations. Regarding that a major fraction of CO_2 was produced during the wetting periods (Fig. 5e), such a lagging effect should be carefully examined when analysing the climatic sensitivity of F_S .

Accounting for the effects of biocrust organisms is also important to accurately estimate C exchanges in dryland ecosystems (Maestre and Cortina, 2003; Castillo-Monroy et al., 2011). Existing studies on the C functioning of biocrust have mainly focused on measuring the net C exchanges under laboratory conditions or from field (e.g., Maestre and Cortina 2003; Wilske et al., 2008; Bowling et al., 2011). However, the contributions of biocrusts as C sink or source remain largely unknown (Castillo-Monroy et al., 2011), due to the difficulty to separate the CO_2 exchanges of crust organisms from the background respirations (Castillo-Monroy et al., 2011; Sancho et al., 2016). In this sense, use of our mechanistic model may provide more insights on the roles of biocrusts in soil C cycling and effluxes. our simulation study showed that the C exchanges of biocrust was largely masked by the background effluxes from root-zone soil. The C uptake by biocrust turned the soil from a net CO_2 source to sink during large rewetting events only, when the background emission was restricted. After rain stopped, the sinks diminished quickly (e.g. within 1 day, Fig. 5b – 5c), not only due to the decreased photosynthesis with drying, but also the increased CO_2 emission from the soil underneath. Based on the climatic variables of a two-year period (Test 4), the simulated NPP of the topcrust was 31 g C m^{-2} $year^{-1}$ at the interspace conditions. Considering a 30% coverage of lichens over the sampling area (Feng et al., 2014), the interspace-level NPP was 9.3 g C m^{-2} $year^{-1}$. This value was largely greater than the lab-based estimation for the site (Feng et al., 2014), but it was in range of the values reported from several other dryland ecosystems (i.e. 5–3 - 29 g C m^{-2} $year^{-1}$, Sancho et al., 2016).

Our simulations also suggested that photodegradation might offset about 48 % of the CO_2 photosynthesized by biocrust and reduced the net sequestration to about 5 gC m^{-2} $year^{-1}$. It could explain the much higher F_S measured from the transparent chamber (C3) than the opaque chamber (C2) during dry daytime periods (e.g. Fig. 8). It should be also noticed that the litter from shrub canopy was not included in the measurement nor modelling. Also, the interactions between photodegradation and biotic decaying were not considered either. Therefore, the contribution of photodegradation to soil C balance could be greater than our estimation at the ecosystem level (see e.g. Gliksman et al., 2016). Future studies are therefore required to clarify the role of photodegradation in regulating the C turnover and sequestration of biocrusts in arid and semiarid ecosystems.

5. Conclusions

This work represents a first attempt to integrate the CO_2 production, transport and surface exchanges (e.g. biocrust photosynthesis, respiration and photodegradation) in F_S modelling for dryland ecosystems of high plant-interspace heterogeneities. Our model simulated reasonably well the F_S dynamics measured from non-crusted and lichen-crusted soil collars during year 2013-2014, although introducing the gas exchanges of lichen crust into modelling decreased the model performance at the hourly scale. Our model could thus be used to simulate the seasonal and annual F_S in dryland soils similar to our site. However, further development of model may still be required on several aspects, e.g. by including. i) the spatial-explicit schemes for surface conditions and soil biogeochemistry; ii) influences of lime and solids on CO_2 transport; iii) growth dynamics of plants; iv) high-resolution dynamics of surface water-thermal conditions and v) the dynamics of microstructure and microbial communities of biocrusts.

Our modelling work also highlighted that, the plant-interspace heterogeneity and complexity of soil C processes could affect largely the soil CO_2 efflux. The presence of plant cover tended to decrease the CO_2 production from root-zone soil probably due to the cooling effect of canopy. Moreover, the transport processes of inorganic C and the metabolisms of biocrusts strongly modified the CO_2 efflux, and these influences are closely linked to soil hydrology. The CO_2 emission from root-zone soil also delayed by increased CO_2 dissolution after rewetting. In addition, an ineligible fraction of respired CO_2 could be removed via lateral flows and root uptakes, and be "missing" from volumes under respiration chambers. During rewetting, the lichen-crusted soil could shift from net CO_2 source to sink, due to the activated photosynthesis of lichens and the restricted CO_2 emissions from subsoil. Whereas after rain events, the NPP of lichens could be easily masked by the background C emissions from the soil profile. Based on our modelling, the annual NPP was 9.3 gC m^{-2} by topcrust at interspace. However, the net C sequestration by topcrust could be marginal, if the photodegradation is accounted.

To conclude, our work suggests that the complexity and plant-interspace heterogeneities of soil C processes affect largely the soil CO_2 efflux dynamics and their climatic sensitivities, which should be carefully considered in extrapolation of findings from chamber to ecosystem level and from seasonal to inter-annual scales. Our model can also serve as a useful tool to simulate the soil CO_2 efflux dynamics in dryland ecosystems.

Acknowledgement

This modelling work was carried out under the Finnish-Chinese research collaboration project EXTREME (2013-2016) by the University of Eastern Finland and Beijing Forestry University. The instrumentation and field measurements utilized in this work were supported by National Natural Science Foundation of China (NSFC) (Proj. No. 31361130340, No. 31670710 and 31670708) and Beijing Forestry University. The modelling work of EXTREME project was supported by the Academy of Finland (proj. no. 14921) and the University of Eastern Finland. Thanks to Peng Liu, Huishu Shi, Yuming Zhang, Sijing Li, Zhihao Chen, Siling Tang, Yajuan Wu and Yuan Li for assistance on the field measurements and instrumentation maintenance.

References

Asaeda, T., Karunaratne, S., 2000. Dynamic modeling of the growth of Phragmites australis: Model description. Aquatic Botany 67, 301–318.

Aguilar, A.J., Huber-Sannwald, E., Belnap, J., Smart, D.R., Moreno, J.T.A., 2009. Biological soil crusts exhibit a dynamic response to seasonal rain and release from grazing with implications for soil stability. Journal of Arid Environment 73, 1158–1169.

Armer, A.M., 2011. Prediction of hydraulic conductivity and sorptivity in soils at steady-state infiltration. Archives of Agronomy and Soil Science 58, doi:10.1080/03650340.2011.572877

Austin, A.T., Vivanco, L., 2006. Plant litter decomposition in a semi-arid ecosystem controlled by photodegradation. Nature 442, 555–558.

Barron-Gafford, G.A., Angert, A.L., Venable, D.L., Tyler, A.P., Gerst, K.L., Huxman, T.E., 2013. Photosynthetic temperature responses of co-occurring desert winter annuals with contrasting resource-use efficiencies and different temporal patterns of resource utilization may allow for species coexistence. Journal of Arid Environments 91, 95-103.

Bégué, A., Hanan, N.P., Prince, S.D., 1994. Radiative transfer in shrub savanna sites in Niger: preliminary results from HAPEX-Sahel. 2. Photosynthetically active radiation interception of the woody layer. Agric. For. Meteorol. 69, 247–266.

Belnap, J., Budel, B., Lange, O.L., 2003. Biological soil crusts: characteristics and distribution. In: Belnap, J., Lange, O.L. (Eds.), Biological Soil Crusts: Structure, Function, and Management, vol. 150. Springer, Berlin, pp. 3–30.

Bloemen, J., McGuire, M.A., Aubrey, D.P., Teskey, R.O., Steppe, K., 2013. Transport of root-derived CO2 via the transpiration stream affects aboveground carbon assimilation and CO_2 efflux in trees. New Phytologist 197, 555–565.

Bloemen, J., Teskey, R.O., McGuire, M.A., Aubrey, D.P., Steppe, K., 2016. Root xylem CO_2 flux: an important but unaccounted-for component of root respiration. Trees 30, 343–352.

Bowling, D.R., Grote, E.E., Belnap, J., 2011. Rain pulse response of soil CO_2 exchange by biological soil crusts and grasslands of the semiarid Colorado Plateau, United States. Journal of Geophysical Research G: Biogeosciences 116, 1–17. doi:10.1029/2011JG001643

Bradford, M.A., Wieder, W.R., Bonan, G.B., Fierer, N., Raymond, P.A., Crowther, T.W., 2016. Managing uncertainty in soil carbon feedbacks to climate change. Nature Climate Change 6, 751–758.

Brandt, L.A., King, J.Y., Hobbie, S.E., Milchunas, D.G., Sinsabaugh, R.L., 2010. The role of photodegradation in surface litter decomposition across a grassland ecosystem precipitation gradient. Ecosystems 13, 765–781.

Buysse, P., Goffin, S., Carnol, M., Malchair, S., Debacq, A., Longdoz, B., Aubinet M., 2013. Short-term temperature impact on soil heterotrophic respiration in limed agricultural soil samples. Biogeochemistry 112, 441–455.

Chamizo, S., Stevens, A., Canton, Y., Miralles, I., Domingo, F., Van Wesemael, B., 2012. Discriminating soil crust type, development stage and degree of disturbance in semiarid environments from their spectral characteristics. Eur. J. Soil Sci. 63, 42–53.

Caylor, K.K., Scanlon, T.M., Rodríguez-Iturbe, I., 2008. Ecohydrological optimizationof pattern and processes in water-limited ecosystems. In: Water and the Environment: Proceedings of the Workshop in the Vatican Academy of Sciences, November 2005. Vatican Academy of Sciences: Vatican Press: TheVatican.

Castillo-Monroy, A.P., Bowker, M.A., Maestre, F.T., Rodríguez-Echeverría, S., Martinez, I., Barraza-Zepeda, C.E., Escolar, C., 2011. Relationships between biological soil crusts, bacterial diversity and abundance, and ecosystem functioning: insights from a semi-arid Mediterranean environment. Journal of Vegetation Sciences 22:165–174

Chen, J.M., Liu, J., Cihlar, J., Goulden, M.L., 1999. Daily canopy photosynthesis modelthrough temporal and spatial scaling for remote sensing applications. Ecological Modelling 124, 99–119.

Chen, X., Duan, Z., 2009. Changes in soil physical and chemical properties during reversal of desertification in Yanchi County of Ningxia Hui autonomous region, China. Environmental Geology 57, 975–985.

Ciais, P., Sabine, C., Bala, G., Bopp, L., Brovkin, V., Canadell, J., Chhabra, A., DeFries, R., Galloway, J., Heimann, M., Jones, C., Le Quéré, C., Myneni, R.B., Piao, S., Thornton, P., France, P.C., Willem, J., Friedlingstein, P., Munhoven, G., 2013. Carbon and other biogeochemical cycles. In: Stocker, T., Qin, D., Plattner, G., Tignor, M., Allen, S., Boschung, J., Nauels, A., Xia, Y., Bex, V., Midgley, P. (Eds.), Climate change 2013—the physical science basis. Cambridge University Press, Cambridge, pp 465–570.

Curiel Yuste, J., Baldocchi, D.D., Gershenson, A., Goldstein, A., Misson, L., Wong, S., 2007. Microbial soil respiration and its dependency on carbon inputs, soil temperature and moisture. Global Change Biology 13, 1–18.

Curiel Yuste, J., Janssens, I.A., Carrara, A., Ceulemans, R., 2004. Annual Q10 of soil respiration reflects plant phenological patterns as well as temperature sensitivity. Global Change Biology 10, 161–169.

Domingo, F., Villagarcía, L., Brenner, A.J., Puigdefábregas, J., 2000. Measuring and modeling the radiation balance of a heterogeneous shrubland. Plant Cell and Environment 23, 27–38.

Donat, M.G., Lowry, A.L., Alexander, L.V., O'Gorman, P.A., Maher, N., 2016. More extreme precipitation in the world's dry and wet regions. Nature Climate Change 6, 508–513.

Emmerich, E.W., 2003. Carbon dioxide flux in a semiarid environment with high carbonate soils. Agricultural and Forest Meteorology 116, 91–102.

Fa, K., Liu, J., Zhang, Y., Wu, B., Qin, S., Feng, W., Lai, Z., 2014. CO_2 absorption of sandy soil induced by rainfall pulses in a desert ecosystem. Hydrological Processes 29, 2043–2051.

Fan, Z., Neff, J.C., Hanan, N.P., 2015. Modeling pulsed soil respiration in an African savanna ecosystem. Agricultural and Forest Meteorology 200, 282–292.

Fang, C., Moncrieff, J.B., 1999. A model for soil CO2 production and transport 1: Model development. Agricultural and Forest Meteorology 95, 225–236.

Felde, V.J.M.N.L., Peth, S., Uteau-Puschmann, D., Drahorad, S.L., Felix-Henningsen, P., 2014. Soil microstructure as an under-explored feature of biological soil crusts hydrological properties: case study from the NW Negev Desert. Biodivers Conserv 23, 1687–1708.

Feng, W., Zhang, Y., Wu, B., Zha, T., Jia, X., Qin, S., Shao, C., Liu,J., Lai, Z., Fa, K., 2013. Influence of disturbance on soil respiration in biologically crusted soil during the dry season, The Scientific World J. doi:10.1155/2013/408560

Feng, W., Zhang, Y., Wu, B., Qin, S., Lai, Z., 2014. Influence of environmental factors on carbon dioxide exchange in biological soil crusts in desert areas. Arid Land Research and Management 28, 186–196.

Evans, S.E., Wallenstein, M.D., 2011. Soil microbial community response to drying and rewetting stress: does historical precipitation regime matter? Biogeochemistry 109, 101–116.

Fu, S., Cheng, W., Susfalk, R., 2002. Rhizosphere respiration varies with plant species and phenology: A greenhouse pot experiment. Plant and Soil 239, 133–140.

Gao, Y., Li, X., Liu, L., Jia, R., Yang, H., Li, G., Wei, Y., 2012. Seasonal variation of carbon exchange from a revegetation area in a Chinese desert. Agricultural and Forest Meteorology 156, 134–142.

Garcia-Pichel, F., Felde, V.J.M.N.L., Drahorad, S., Weber, B., 2016. Microstructure and weathering processes within biological soil crusts. In: Weber, B., Büdel, B., Belnap, J. (Eds.), Biological soil crusts: an organizing principle in drylands. Springer, Switzerland, pp 237–252.

Garcia-Pichel, F., Pringault, O., 2001. Microbiology—cyanobacteria track water in desert soils. Nature 413, 380–381.

Giardina, C.P., Litton, C.M., Crow, S.E., Asner, G.P., 2014. Warming-related increases in soil CO2 efflux are explained by increased below-ground carbon flux. Nature Climate Change 4, 822–827.

Gliksman, D., Rey, A., Seligmann, R., Dumbur, R., Sperling, O., Navon, Y., Haenel, S., Angelis, P.D., Arnone III, J.A., Grünzweig, J.M., 2016. Biotic degradation at night, abiotic degradation at day: positive feedbacks on litter decomposition in drylands. Global Change Biology, doi: 10.1111/gcb.13465.

Gong, J., Kellomäki, S., Shurpali, N.J., Wang, K., Hyvönen, N., Zhang, C., Zhong, Q., Martikainen, P.J., 2014. Climatic sensitivity of the CO_2 flux in a cutaway boreal peatland cultivated with a perennial bioenergy crop (*Phalaris arundinaceae, L.*): Beyond diplotelmic modeling. Agricultural and Forest Meteorology 198-199, 232-249.

Gong, J., Kellomäki, S., Wang, K., Zhang, C., Shurpali, N., Martikainen, P.J., 2013. Modeling CO_2 and CH_4 flux changes in pristine peatlands of Finland underchanging climate conditions. Ecological Modelling 263, 64–80.

Gong, J., Jia, X., Zha, T., Wang, B., Kellomäki, S., Peltola, H., 2016. Modelling the effects of plant-interspace heterogeneity on water-energy balances in a semiarid ecosystem. Agricultural and Forest Meteorology 221, 189–206.

Green, T.G.A., Proctor, M.C.F., 2016. Physiology of photosynthetic organisms within biological soil crusts: Their adaptation, flexibility, and plasticity. In: Weber, B., Büdel, B., Belnap, J. (Eds.), Biological soil crusts: an organizing principle in drylands. Springer, Switzerland, pp 347–384.

Henry, H.A.L., Brizgys, P., Field, C.B., 2008. Litter decomposition in California annual grassland: interactions between photodegradation and litter layer thickness. Ecosystems 11, 545–554.

Jarvis, P., Rey, A., Petsikos, C., Wingate, L., Rayment, M., Pereira, J., Banza, J., David, J., Miglietta, F., Borghetti, M., Manca, G., Valentini, R., 2007. Drying and wetting of Mediterranean soils stimulates decomposition and carbon dioxide emission: the "Birch effect". Tree Physiology 27, 929-40.

Jia, R.L., Li, X.R., Liu, L.C., Gao, Y.H., Li, X.J., 2008. Responses of biological soil crusts to sand burial in a revegetated area of the Tengger desert, northern china. Soil Biology and Biochemistry 40:2827–2834

Jia, X., Zha, T.S., Wu, B., Zhang, Y.Q., Gong, J.N., Qin, S.G., Chen, G.P., Qian, D.,Kellomäki, S., Peltola, H., 2014. Biophysical controls on net ecosystem CO2exchange over a semiarid shrubland in northwest China. Biogeosciences 11, 4679–4693.

Jia, X., Zha, T.S., Gong, J.N., Wu, B., Zhang, Y.Q., Qin, S.G., Chen, G.P., Feng, W.,Kellomäki, S., Peltola, H., 2015. Energy partitioning over a semi-arid shrubland in northern China. Hydrological Processes http://dx.doi.org/10.1002/hyp.10685.

Jia, X., Zha, T.S., Gong, J., Wang, B., Zhang, Y., Wu, B., Qin, S, Peltola, H., 2016. Carbon and water exchange over a temperate semi-arid shrub land during three years of contrasting precipitation and soil moisture patterns. Agricultural and Forest Meteorology 228, 120–129.

Karhu, K., Auffret, M.D., Dungait, J.A.J., Hopkins, D.W., Prosser, J.I., Singh, B.K., Subke, J.-A., Wookey, P.A., Ågren, G.I., Sebastià, M.-T., Gouriveau, F., Bergkvist, G., Meir, P., Nottingham, A.T., Salinas, N., Hartley, L.P., 2014. Temperature sensitivity of soil respiration rates enhanced by microbial community response. Nature 513, 81–84.

Kinast, S., Ashkenazy, Y., Meron, E., 2014. A coupled vegetation-crust model for patchy landscapes. Pure and Applied Geophysics 173, 1-11.

Lai, Z., Zhang, Y., Liu, J., Wu, B., Qin, S., Fa, K., 2015. Fine-root distribution, production, decomposition, and effect on soil organic carbon of three revegetation shrub species in northwest China. Forest Ecology and Management 359, 381-388.

Lange, O.L., 2003. Photosynthetic productivity of the epilithic lichen *Lecanora muralis*: long-term field monitoring of CO2 exchange and its physiological interpretation. III. Diel, seasonal, and annual carbon budgets. Flora 198, 277–292.

Biogeosciences Discuss., doi:10.5194/bg-2017-95, 2017
Manuscript under review for journal Biogeosciences
Discussion started: 4 April 2017

Li, Y., Wang, Y., Houghton, R.A., Tang, L., 2015. Hidden carbon sink beneath desert. Geophysical Research Letters 42, 5880–5887.

Liu, J., Zhang, Y., Wu, B., Qin, S., Jia, X., Fa, K., Feng, W., Lai, Z., 2015. Effect of vegetation rehabilitation on soil carbon and its fractions in Mu Us desert, northwest China. International Journal of Phytoremediation 17, doi:10.1080/15226514.2014.922923

Liu, L.C., Li, S.Z., Duan, Z.H., Wang, T., Zhang, Z.S., Li, X.R., 2006. Effects of microbiotic crusts on dew deposition in the restored vegetation area at Shapotou, northwestern China. Journal of Hydrology 328, 331–337.

Liu, P., Zha, T., Jia, X., Wang, B., Guo, X., Zhang, Y., Wu, B., Yang, Q., Peltola, H., 2016. Diurnal freeze-thaw cycles modify winter soil respiration in a desert shrub-land ecosystem. Forests 7, doi:10.3390/f7080161

Ma, Q., Cheng, F., Liu, Y., Wang, F., Zhang, D., Jin, H., 2011. Spatial heterogeneity ofsoil water content in the reversion process of desertification in arid areas. Journal of Arid Land 3, 268–277.

Ma, J., Wang, Z.Y., Stevenson, B.A., Zheng, X.J., Li, Y., 2013. An inorganic CO_2 diffusion and dissolution process explains negative CO2 fluxes in saline/alkaline soils. Scientific Report 3, doi: 10.1038/srep02025.

Maier, M., Schack-Kirchner, H., Hildebrand, E.E., Schindler, D., 2011. Soil CO_2 efflux vs. soil respiration: Implications for flux models. Agricultural and Forest Meteorology 151, 1723–1730.

Maestre, F.T., Cortina, J., 2003. Small-scale spatial variation in soil CO2 efflux in a Mediterranean semiarid steppe. Applied Soil Ecology 23, 199–209.

Maestre, F.T., Escolar, C., Bardgett, R.D., Dungait, J.A., Gozalo, B., Ochoa, V., 2015. Warming reduces the cover and diversity of biocrust-forming mosses and lichens, and increases the physiological stress of soil microbial communities in a semi-arid *Pinus halepensis* plantation. Front Microbial. 6, doi:10.3389/fmicb.2015.00865

Maestre, F.T., Escolar, C., Ladrón de Guevara, M., 2013. Changes in biocrust cover drive carbon responses to climate change in drylands. Global Change Biology 19, 3835–3847.

Rietkerk, M., Dekker, S.C., de Ruiter, P.C., van de Koppe, J., 2004. Self-organizedpatchiness and catastrophic shifts in ecosystems. Science 305, 1926–1929.

Reynolds, J.F., Virginia, R.A., Kemp, P.R., de Soyza, A.G., Tremmel, D.C., 1999. Impact of drought on desert shrubs: effects of seasonality and degree of resource island development. Ecol. Monogr. 69, 69–106.

Biogeosciences Discuss., doi:10.5194/bg-2017-95, 2017
Manuscript under review for journal Biogeosciences
Discussion started: 4 April 2017

Phillips, C.L., Nickerson, N., Risk, D., Bond, B.J., 2011. Interpreting diel hysteresis between soil respiration and temperature. Global Change Biology 17, 515–527.

Pointing, S.B., Belnap, J., 2012. Microbial colonization and controls in dryland systems. Nature Review Microbiology 10, 551–562.

Rango, A., Tartowskia, S.L., Laliberte, A., Wainwright, J., Parsons, A., 2006. Islands of hydrologically enhanced biotic productivity in natural and managed arid ecosystems. J. Arid Environ. 65, 235–252.

Porada, P., Weber, B., Elbert, W., Pöschl, U., Kleidon, A., 2013. Estimating global carbon uptake by lichens and bryophytes with a process-based model. Biogeosciences 10, 6989–7033.

Poulter, B., Frank, D., Ciais, P., Myneni, R. B., Andela, N., Bi, J., Broquet, G., Canadell, J. G., Chevallier, F., Liu, Y. Y., Running, S. W., Sitch, S., van der Werf, G.R., 2014. Contribution of semiarid ecosystems to interannual variability of the global carbon cycle. Nature, 509, 600–603.

Qi, F., Kunihikow, E., Guodong C., 2002. Soil water and chemical characteristics of sandy soils and their significance to land reclamation. Journal of Arid Environments 51, 35–54.

Raanan, H., Felde, V.J.M.N.L., Peth, S., Drahorad, S., Ionescu, D., Eshkol, G., Treves, H., Felix-Henningsen, P., Berkowicz, S., Keren, N., Horn, R., Hagemann, M., Kaplan, A., 2016. Three-dimensional structure and cyanobacterial activity within a desert biological soil crust. Environ Microbiol 18, 372–383. doi:10.1111/1462-2920.12859

Raich, J.W., Tufekciogul, A., 2000. Vegetation and soil respiration: correlations and controls. Biogeochemistry 48, 71-90.

Raich, J.W., Potter, C.S., Bhagawati, D., 2002. Interannual variability in global soil respiration, 1980–94. Global Change Biology 8, 800–812.

Rastud, L.E., Huntington, T.G., Boone, R.D., 2000. Controls on soil respiration: implications for climate change. Biogeochemistry 48, 1–6.

Rey, A., Petsikos, C., Jarvis, P.G., Grace, J., 2005. Effect of temperature and moisture on rates of carbon mineralization in a Mediterranean oak forest soil under controlled and field conditions. European Journal of Soil Science 56, 589–599.

Reynolds, J.F., Virginia, R.A., Kemp, P.R., de Soyza, A.G., Tremmel, D.C., 1999. Impact of drought on desert shrubs: effects of seasonality and degree of resource island development. Ecol. Monogr. 69, 69–106.

Rietkerk, M., Dekker, S.C., de Ruiter, P.C., van de Koppe, J., 2004. Self-organized patchiness and catastrophic shifts in ecosystems. Science 305, 1926–1929.

Biogeosciences Discuss., doi:10.5194/bg-2017-95, 2017
Manuscript under review for journal Biogeosciences
Discussion started: 4 April 2017

Rodríguez-Iturbe, I., Porporato, A., Laio, F., Ridolfi, L., 2001. Plants in water-controlled ecosystems: active role in hydrologic processes and response to water stress—i. Scope and general outline. Advances in Water Resources 24, 695–705.

Rango, A., Tartowskia, S.L., Laliberteа, A., Wainwright, J., Parsons, A., 2006. Islandsof hydrologically enhanced biotic productivity in natural and managed aridecosystems. J. Arid Environ. 65, 235–252.

Ryan, M.G., Law, B.E., 2005. Interpreting, measuring, and modeling soil respiration. Biogeochemistry 73, 3–27.

Sala, O.E., Gherardi, L.A., Reichmann, L., Jobbágy, E., Peters, D., 2012. Legacies of precipitation fluctuations on primary production: theory and data synthesis. Philos. T. Roy. Soc. B. 367, 3135–3144.

Sancho, L.G., Belnap, J., Colesie, C., Raggio, J., Weber, B., 2016. Carbon budgets of biological soil crusts at micro-, meso-, and global scales. In: Weber, B., Büdel, B., Belnap, J. (Eds.), Biological soil crusts: an organizing principle in drylands. Springer, Switzerland, pp 287–304.

Schlesinger, W.H., Belnap, J., Marion, G., 2009. On carbon sequestration in desert ecosystems. Global Change Biology 15, 1488–1490.

Shen, W., Jenerette, G.D., Hui, D., Scott, R.L., 2016. Precipitation legacy effects on dryland ecosystem carbon fluxes: direction, magnitude and biogeochemical carryovers. Biogeosciences 13, 425–439.

Šimunek, J., Suarez, D.L., 1993. Modeling of carbon dioxide transport and production in soil: 1. Model development. Water Resources Research 29, 487–497.

Smith, J.U., Gottschalk, P., Bellarby, J., Chapman, S., Lilly, A., Towers, W., Bell, J., Coleman, K., Nayak, D., Richards, M., Hillier, J., Flynn, H., Wattenbach, M., Aitkenhead, M., Yeluripati, J., Farmer, J., Milne, R., Thomson, A., Evans, C., Whitmore, A., Falloon, P., Smith, P., 2010. Estimating changes in national soil carbon stocks using ECOSSE-a new model that includes upland organic soils. Part I. Model description and uncertainty in national scale simulations of Scotland. Climate Research, 45, 179–192.

Shi, R., Yang, X., Zhang H., Wang, L., 2013. Vertical differentiation analysis of sierozem profile characteristics in Yili-River valley, China. African Journal of Agricultural Research 8, 6509–6517.

Song, W.M., Chen, S., Zhou, Y., Wu, B., Zhu, Y., Lu, Q., Lin, G., 2015. Contrasting diel hysteresis between soil autotrophic and heterotrophic respiration in a desert ecosystem under different rainfall scenarios. Scientific Report 5, doi:10.1038/srep16779

Vanderbilt, K.L., White, C.S., Hopkins, O., Craig, J.A., 2008. Aboveground decomposition in arid environments: results of a long-term study in central New Mexico. Journal of Arid Environments 72, 696–709.

van Gestel, N., Reischke ,S., Bååth, E., 2013. Temperature sensitivity of bacterial growth in a hot desert soil with large temperature fluctuations. Soil Biology & Biochemistry 65, 180-185.

Viterbo, P., Beljaars, A., Mahfouf, J., Teixeira, J., 1999. The representation of soil moisture freezing and its impact on the stable boundary layer. Q. J. R. Meteorol. Soc. 125, 2401–2426.

Wang, B., Zha, T.S., Jia, X., Wu, B., Zhang, Y.Q., Qin, S.G., 2014a. Soil moisture modifies the response of soil respiration to temperature in a desert shrub ecosystem. Biogeosciences 11, 259–268.

Wang, W., Chen, Xi., Luo, G., Li, L., 2014b. Modeling the contribution of abiotic exchange to CO_2 flux in alkaline soil of arid areas. Journal of Arid Land 6, 27–36.

Wang, B., Zha, T.S., Jia, X., Gong, J.N., Wu, B., Bourque, C.P.A., Zhang, Y., Qin, S.G., Chen, G.P., Peltola, H., 2015. Microtopographic variation in soil respiration and its controlling factors vary with plant phenophases in a desert-shrub ecosystem. Biogeosciences 12, 5705–5714.

Williams, A.J., Buck, B.J., Beyene, M.A., 2012. Biological soil crusts in the Mojave desert, USA: micromorphology and pedogenesis. Soil Science Society of America Journal 76, 1685–1695.

Xie, J.X., Li, Y., Zhai, C.X., Lan, Z., 2009. CO_2 absorption by alkaline soils and its implication to the global carbon cycle. Environmental Geology 56, 953–961.

Xu, L., Baldocchi, D., Tang, J., 2004. How soil moisture, rain pulses, and growth alter the response of ecosystem respiration to temperature. Global Biogeochemical Cycles 18, doi: 10.1029/2004GB00228.

Yanai, R., 1994. A steady-state model of nutrient uptake accounting for newly grown roots. Soil. Sci. Soc. Am. J. 58, 1562-1571.

Zaady, E., Kuhn, U., Wilske, B., Sandoval-Soto, L., Kesselmeier, J., 2000. Patterns of CO_2 exchange in biological soil crusts of successional age. Soil Biology and Biochemistry 32, 959–966.

Zhang, J., Hou, P., 2012. Changes in soil properties during reversal of desertification in agro-pastoral transition zone of Northern China. African Journal of Agricultural Research 7, 3284-3292.

Zhang, Z.S., Li, X.R., Wang, T., Wang, X.P., Xue, Q.W., Liu, L.C., 2008. Distribution and seasonal dynamics of roots in a revegetated stand of *Artemisia ordosica* Kracsh. in the Tengger Desert (North China). Arid Land Res. Manag. 22, 195–211.

Biogeosciences Discuss., doi:10.5194/bg-2017-95, 2017
Manuscript under review for journal Biogeosciences
Discussion started: 4 April 2017

Tables

Table 1. Configuration of soil collars used in this study

Collars	C1	C2	C3
Surface type	Non-crusted	Lichen-crusted	Lichen-crusted
Chamber type	Opaque	Opaque	Transparent
Root biomass (g m^{-3})	420	106	92
Gap of data (%)	12.9	10.5	9.85
Annual C efflux (gC m^{-2}) [a]	259	194	192

[a] The values were calculated from the measured hourly FS data excluding data gaps.

Table 2. Parameters for soil water retention and C turnover

Parameter	Equation	Unit	Value
α_h	- [a]	-	0.0355 [b]
n	- [a]	-	1.5215 [b]
k_1	(11)	g g^{-1} day^{-1}	0.01 [c]
k_2	(11)	g g^{-1} day^{-1}	0.08 [d]
k_3	(11)	g g^{-1} day^{-1}	0.001 [d]
k_g	(15)	g g^{-1}	0.15 [e]
k_{cr}	(19)	g g^{-1} s^{-1}	0.0014 [f]
k_{R0}	(25)	g g^{-1} day^{-1}	0.002 [e]
a	(26)	-	0.1 [g]
b	(26)	-	24 [g]
c	(26)	-	0.89 [g]
Q_{Ct}	(32)	-	1.585 [f]
a_{RC}	(32)	-	-0.0525 [f]
b_{RC}	(32)	-	2.602 [f]
c_{RC}	(32)	-	-1.653 [f]
a_{Pt}	(33)	-	0.9837 [f]
b_{Pt}	(33)	-	-0.1385 [f]
c_{Pt}	(33)	-	0.0095 [f]
d_{Pt}	(33)	-	-1.6318E-4 [f]
a_{Pw}	(33)	-	-0.3501 [f]
b_{Pw}	(33)	-	5.5884 [f]
c_{Pw}	(33)	-	-7.1783 [f]
d_{Pw}	(33)	-	2.6837 [f]

[a] See Eq. (26) in Gong et al. (2016). Sources of parameter values: [b] This study, see section 2.3.2; [c] Lai et al. (2015); [d] Gong et al. (2014); [e] Chen et al. (1999); [f] This study, see section 2.3.4 and Fig. 2; [g] Wang et al., 2014a.

Biogeosciences Discuss., doi:10.5194/bg-2017-95, 2017
Manuscript under review for journal Biogeosciences
Discussion started: 4 April 2017

Table 3. Simulated annual F_S (gC m^{-2} year^{-1}) and its componential fluxes (gC m^{-2} year^{-1}) at plant cover and interspace

Surface type	F_S	F_T	R_P [a]	Ra	P_{Ct}	F_{Ct}	F_P	F_{Cnet} [b]
Interspace	244	249	295	113	54.6	31.1	26.1	5.0
Plant covered	214	218	263	108	36.3	18.2	14.6	3.6

[a] R_P is the total respired CO_2 in root-zone soil and is the sum of autotrophic respiration ($Ra = \sum_i Ra_i$, see Eq. (10)) and heterotrophic respiration($Rs=\sum_i Rs_i$, see Eq. (12)); [b] F_{Cnet} is the net CO2 exchanges of topcrust and F_{Cnet}= F_{Ct} - F_P, see Eq. (17) – Eq. (18).

Table 4. Sensitivity of simulated F_S and its componential fluxes to changes in parameter values

Change of parameter	F_S	F_T	R_P	Ra	P_{Ct}	F_{Ct}	F_P	F_{Cnet}
n_R +20 %	+3.3	+3.2	+2.7	+7.9	/	/	/	/
n_R -20 %	-2.9	-2.8	-3.4	-8.8	/	/	/	/
n_P +20 %	+1.6	+1.6	+1.0	/	/	/	/	/
n_P -20 %	/	/	-1.4	/	/	/	/	/
f_m +20 %	/	/	/	/	+2.9	+3.8	+3.4	+6.0
f_m -20 %	/	/	/	/	+1.2	/	-5.7	+30
Ts +2 ºC	+9.5 [a]	+9.6	+7.1	+11	+4.9	+3.9	+1.5	+16
Ts -2 ºC	-9.0	-9.2	-8.1	-11	-1.3	-2.9	/ [b]	-20
θ +10 %	+3.6	+5.6	+7.5	+14	+41	+28	+14	+102
θ -10 %	-5.0	-5.6	-8.1	-14	-16	-13	-8.4	-34
M_{tot} +10 %	+2.9	+2.8	+2.0	/	/	/	/	/
M_{tot} -10 %	-2.5	-2.4	-3.1	/	/	/	/	/
M^R +10 %	+7.0	+6.8	+6.8	+8.8	/	/	/	/
M^R -10 %	-7.0	-6.8	-7.1	-8.9	/	/	/	/
N_{tot} +10 %	/	/	/	/	/	/	/	/
N_{tot} -10 %	/	/	/	/	/	/	/	/
k_1 +10 %	+2.9	+2.8	+2.4	/	/	/	/	/
k_1 -10 %	-2.5	-2.4	-3.1	/	/	/	/	/
k_{mo} +10 %	+4.1	+4.0	+3.4	/	/	/	/	/
k_{mo} -10 %	-3.3	-3.2	-3.7	/	/	/	/	/
k_{mc} +10 %	/	/	/	/	/	/	+1.5	-8.0
k_{mc} -10 %	/	/	/	/	/	/	-2.3	+8.0
M_{Ct} +10 %	/	/	/	/	/	/	/	/
M_{Ct} -10 %	/	/	/	/	/	/	/	/
M_{CA}:M_{CH} +10 %	/	/	/	/	/	/	/	/
M_{CA}:M_{CH} -10 %	/	/	/	/	/	/	/	/
pH +5 %	-8.6	-8.4	/	/	/	/	/	/
pH -5 %	+7.0	+6.8	/	/	/	/	/	/

[a] Percentage (%) of changes in the C flux after manipulation of parameter values, as compared to the "base" conditions (i.e. Test 4; see Table 3). All the tests were based on the interspace conditions. [b] The change in the simulated C flux was smaller than 1 % .

Biogeosciences Discuss., doi:10.5194/bg-2017-95, 2017
Manuscript under review for journal Biogeosciences
Discussion started: 4 April 2017

Figures

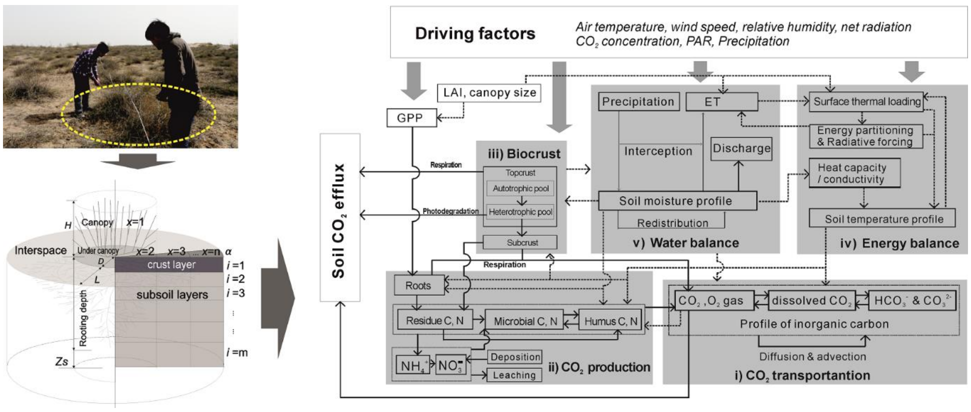

Figure 1. Layout for the setting of representative land unit (RLU, as adopted from Gong et al., 2016) and conceptual framework of process-based modelling

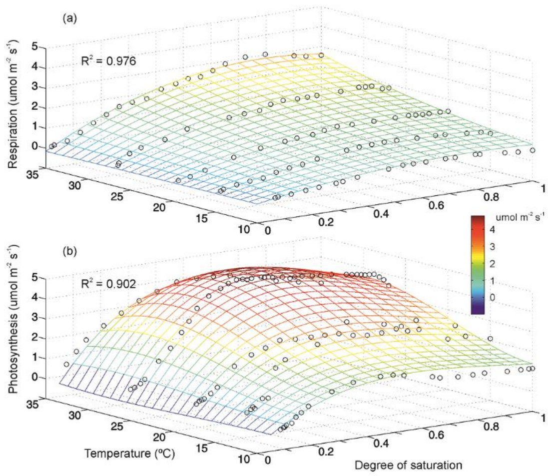

Figure 2. Measured and fitted bulk respiration (a) and photosynthesis (b) of the lichen topcrust as functions of temperature and water content.

Biogeosciences Discuss., doi:10.5194/bg-2017-95, 2017
Manuscript under review for journal Biogeosciences
Discussion started: 4 April 2017

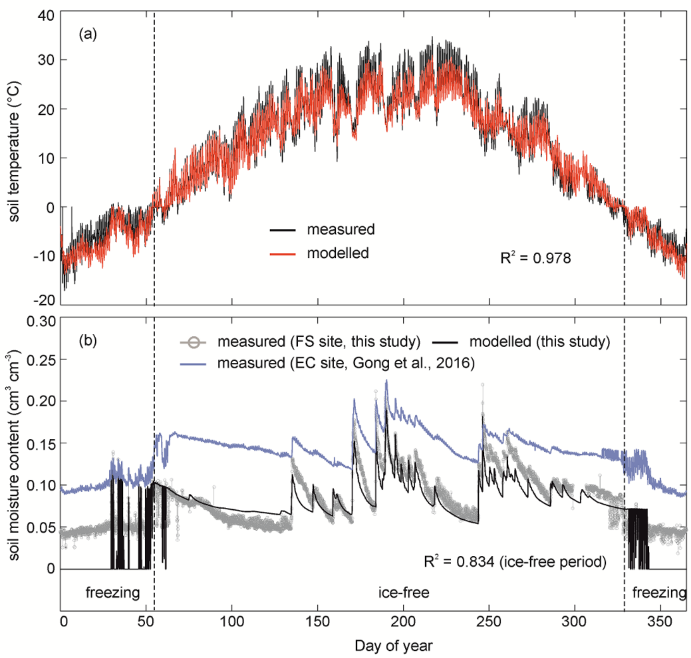

Figure 3. Measured and modelled soil temperature (a) and soil moisture content (b) at 10 cm depth for F_S site, and as compared to the EC site in year 2013 by Gong et al. (2016).

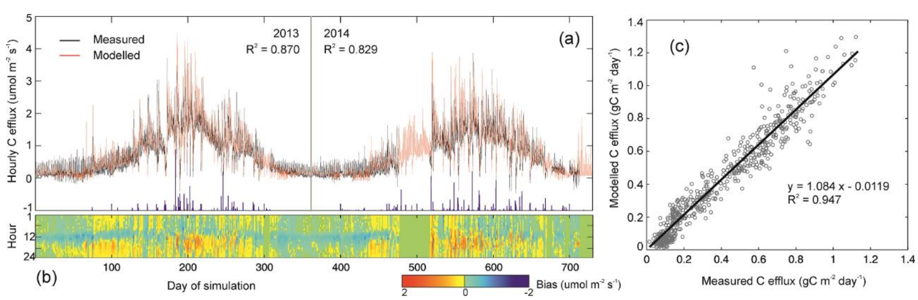

Figure 4. Measured and modelled hourly F_S for non-crusted soil (a), the temporal pattern of the bias of simulated hourly F_S (b) and the comparison of measured and modelled daily F_S (c) during 2013-2014.

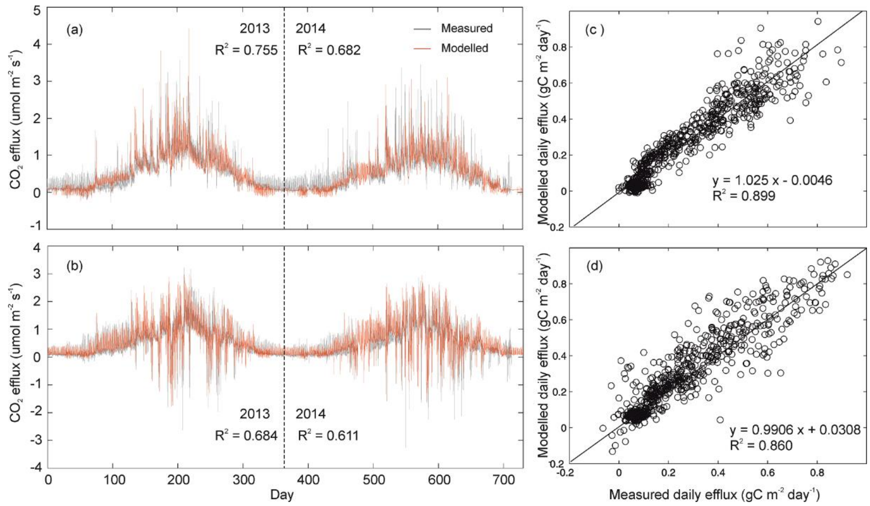

Figure 5. Measured and modelled F_S of lichen-crusted soils for opaque (a, c) and transparent chambers (b, d) at hourly (a, b) and daily (c, d) scales during 2013-2014.

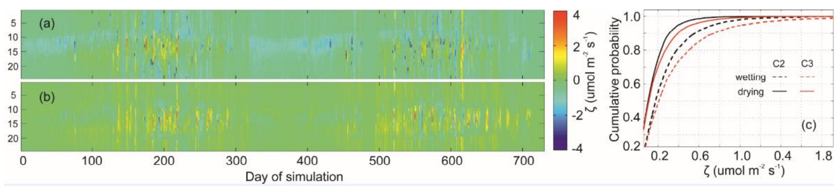

Figure 6. Diurnal patterns of biases in the simulated hourly F_S for lichen-crusted soils using opaque (a) and transparent chambers (b), and the cumulative probability of the biases during wetting and drying periods (c) during 2013-2014. The wetting period included the raining days and a 1-day period after each rainfall. The drying period included the rest time of the years other than the wetting period.

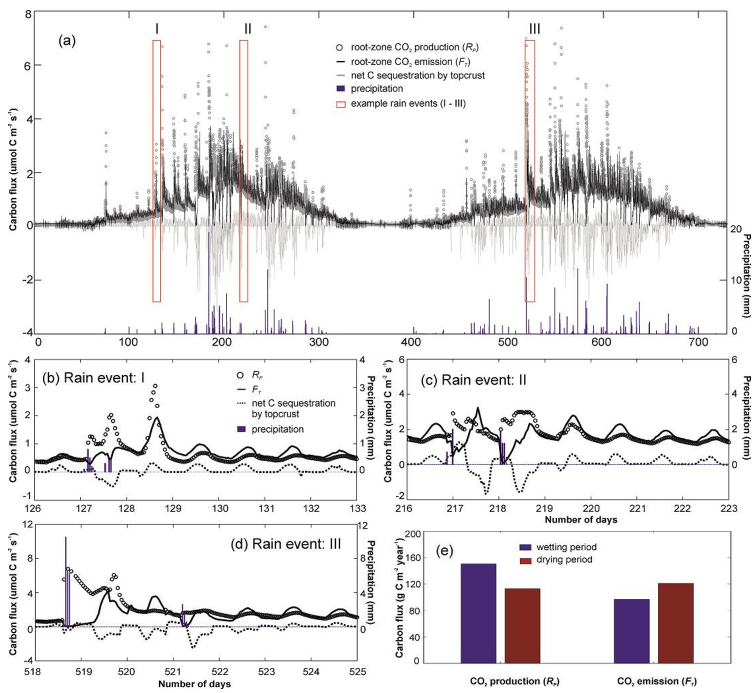

Figure 7. Simulated F_S and CO_2 exchanges by biocrust and root-zone soil (a), the simulated CO_2 fluxes before and after example rain events of 2.3 mm (b), 7.6 mm (c) and 12.8 mm (d) sizes, and the comparison of F_T and R_R during wetting and drying periods during 2013-2014. The wetting period included the raining days and a 1-day period after each rainfall. The drying period included the rest time of the years other than the wetting period.

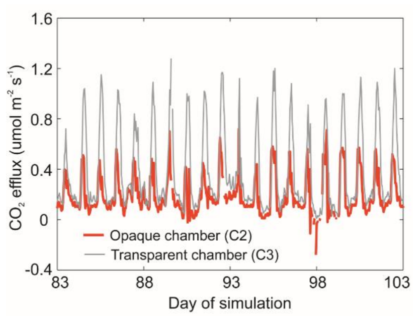

Figure 8. Comparison of the measured F_S from lichen-crusted surfaces using opaque and transparent chambers during a dry period (day 83-103) in spring 2013.